https://doi.org/10.5194/acp-2022-85
Preprint. Discussion started: 4 February 2022

Atmospheric Chemistry and Physics Discussions

Identification of highly oxygenated organic molecules and their role in aerosol formation in the reaction of limonene with nitrate radical

Yindong Guo[1], Hongru Shen[1], Iida Pullinen[2, a], Hao Luo[1,3], Sungah Kang[2], Luc Vereecken[2], Hendrik Fuchs[2], Mattias Hallquist[4], Ismail-Hakki Acir[2,b], Ralf Tillmann[2], Franz Rohrer[2], Jürgen Wildt[2], Astrid Kiendler-Scharr[2], Andreas Wahner[2], Defeng Zhao[1,5,6*], Thomas F. Mentel[2*]

[1]Department of Atmospheric and Oceanic Sciences & Institute of Atmospheric Sciences, Fudan University, 200438, Shanghai, China
[2]Institute of Energy and Climate Research, IEK-8: Troposphere, Forschungszentrum Jülich, 52425, Jülich, Germany
[3]IRDR ICoE on Risk Interconnectivity and Governance on Weather/Climate Extremes Impact and Public Health, Fudan University, Shanghai 200438, China
[4]Department of Chemistry and Molecular biology, University of Gothenburg, Göteborg, 41258, Sweden
[5]Shanghai Frontiers Science Center of Atmosphere-Ocean Interaction, Fudan University, Shanghai 200438, China
[6]Institute of Eco-Chongming (IEC), 20 Cuiniao Rd., Chongming, Shanghai, 202162, China
[a] Now at: Department of Applied Physics, University of Eastern Finland, Kuopio, 70210, Finland.
[b] Now at: Institute of Nutrition and Food Sciences, University of Bonn, Bonn, 53115, Germany.
Correspondence to: Defeng Zhao (dfzhao@fudan.edu.cn), Thomas F. Mentel (t.mentel@fz-juelich.de)

Abstract. Nighttime nitrate radical(NO_3)-initiated oxidation of biogenic volatile organic compounds (BVOC) such as monoterpenes is important for the formation and growth of secondary organic aerosol (SOA), which has significant impact on climate, air quality and human health. In SOA formation and growth from the oxidation of monoterpenes by NO_3, highly oxygenated organic molecules (HOM) may be crucial, but their formation pathways and role in aerosol formation have yet to be clarified. Among monoterpenes, limonene is of research interest for its high emission globally and high SOA yield. In this work, HOM formation in the reaction of limonene with nitrate radical was investigated in the SAPHIR chamber (Simulation of Atmospheric PHotochemistry In a large Reaction chamber). About 280 HOM products were identified, grouped into 6 monomer series (each including 3 families) and one family, 11 dimer families and 3 trimer families. Both closed-shell products and open-shell peroxy radicals (RO_2•) were observed, and many of them have not been reported previously. Monomers and dimers accounted for over 90 % of HOM concentrations. In the most abundant monomer series – $C_{10}H_{15\text{-}17}NO_{6\text{-}14}$, carbonyl products outnumbered hydroxyl products, indicating the importance of the unimolecular RO_2• termination pathway. Both RO_2• autoxidation and alkoxy-peroxy pathways were found to be important processes leading to HOM. Time-dependent concentration profiles of monomer products containing nitrogen showed mainly second-generation formation patterns. Dimers were likely formed via the accretion reaction of two monomer RO_2•, and HOM-trimers via the accretion reaction between

https://doi.org/10.5194/acp-2022-85
Preprint. Discussion started: 4 February 2022

Atmospheric Chemistry and Physics Discussions

monomer RO_2• and dimer RO_2•. Trimers are suggested to play an important role in new particle formation (NPF) observed in our experiment. A HOM yield of 1.5 % (+1.7 %/-0.7 %) was estimated considering only first-generation products. SOA mass growth could be reasonably explained by HOM condensation on particles assuming irreversible uptake of extremely low volatility organic compounds (ELVOC) and low volatility organic compounds (LVOC). This work provides evidence for the important role of HOM formed via the limonene + NO_3 reaction in NPF and SOA growth.

1 Introduction

The nitrate radical (NO_3) is an important nighttime oxidant in tropospheric chemistry, and can reach mixing ratios of several hundred pptv during nighttime (Seinfeld and Pandis, 2006). It can react with volatile organic compounds (VOC) and is especially reactive to alkenes, where a nitrate group can be added to C=C double bond through addition reaction (Finlayson-Pitts and Pitts, 1997; Seinfeld and Pandis, 2006). Biogenic monoterpene ($C_{10}H_{16}$) is a large source of alkenes in the atmosphere (Klinger et al., 2002; Guenther et al., 2012), and its major nighttime loss pathway is reacting with NO_3 (Beaver et al., 2012; Rollins, 2012; Ayres et al., 2015; Fry et al., 2013). The chemistry of monoterpenes with NO_3 has implications on the cycle of reactive nitrogen and thus on ozone formation. Since the NO_3 radical is formed through the reaction of NO_2 with O_3, it is considered to be anthropogenic origin, and reactions of NO_3 with biogenic VOC (BVOC) represent a typical interaction between biogenic emissions and anthropogenic emissions.

The reaction of NO_3 with monoterpenes can also form secondary organic aerosols (SOA), which can have a large impact on global climate, air quality and human health (Hallquist et al., 2009; Shrivastava et al., 2017). Laboratory studies showed that monoterpenes have high SOA yields in the reaction with NO_3 due to the low volatility of oxidation products (Ng et al., 2008; Rollins et al., 2009; Fry et al., 2013; Fry et al., 2014; Ayres et al., 2015; Jokinen et al., 2015; Zhou et al., 2015; Boyd et al., 2015; Nah et al., 2016; Boyd et al., 2017; Slade et al., 2017; Claflin and Ziemann, 2018). Field studies also showed that nighttime NO_3-initiated oxidation of monoterpenes contributes significantly to SOA in forested regions influenced by anthropogenic emissions (Pye et al., 2010; Rollins, 2012; Fry et al., 2013; Ayres et al., 2015; Zhou et al., 2015; Xu et al., 2015; Lee et al., 2016; Zhang et al., 2018; Chen et al., 2020) and potentially in urban areas due to the usage of volatile chemical products (VCP) (Nazaroff and Weschler, 2004; Mcdonald et al., 2018). For example, the Southern Oxidant and Aerosol Study (SOAS) showed that the BVOC + NO_3 reactions were a substantial source of SOA (Ayres et al., 2015; Xu et al., 2015; Lee et al., 2016; Massoli et al., 2018). Therefore, accurate predictions and evaluations of SOA concentration and thus its climate and environmental

https://doi.org/10.5194/acp-2022-85
Preprint. Discussion started: 4 February 2022


Atmospheric Chemistry and Physics Discussions

effects require a comprehensive understanding of the reactions of monoterpenes with NO_3.

Among all species of monoterpenes, understanding the reaction system of limonene with NO_3 is of special importance. The emission of limonene makes the 4th largest contribution with an estimated global emission of 11.4 Tg annually, preceded only by α-pinene, t-β-ocimene and β-pinene (Guenther et al., 2012). Besides its biogenic origin, limonene is a common additive in cleaning products (Nazaroff and Weschler, 2004) and can be used as a tracer for fragrances in some places (Gkatzelis et al., 2021). Several studies have shown adverse health effects due to indoor pollution caused by the ozonolysis of limonene (Clausen et al., 2001; Fan et al., 2003; Carslaw et al., 2012; Pagonis et al., 2019). Moreover, limonene stands out with its high reactivity towards the NO_3 radical (with a lifetime of 3 min at 298 K at 20 pptv NO_3) (Ziemann and Atkinson, 2012), and NO_3 oxidation of limonene has high SOA yield (SOA mass yield 15 to 231 %) (Hallquist et al., 1999; Spittler et al., 2006; Fry et al., 2011; Fry et al., 2014; Boyd et al., 2017; Berkemeier et al., 2020; Mutzel et al., 2021). A number of studies have provided valuable insights into the reaction of limonene with NO_3 regarding its SOA yield, main products and their formation pathways as well as the physicochemical properties of SOA (Peng et al., 2018). For example, Hallquist et al. (1999) measured the SOA mass yield and revealed the dominance of organic nitrates (ON) and carbonyl compounds in the products. Fry et al. (2011) determined the organic nitrate yield and proposed a reaction scheme leading to the formation of organic nitrates and carbonyls, and Fry et al. (2014) compared the SOA and ON yields from the NO_3 oxidation of α-pinene, β-pinene, and limonene, and demonstrated why limonene + NO_3 leads to more SOA and ON than α-pinene from a structural perspective. Boyd et al. (2017) found a higher N:C ratio of limonene + NO_3 SOA than β-pinene + NO_3 SOA. Theoretical investigations have revealed that NO_3 addition on the endocyclic C=C double bond is more favorable than the exocyclic one due to a lower energy barrier (Jiang et al., 2009). Typically, in the limonene + NO_3 reaction, the endocyclic double bond of limonene tends to be attacked by NO_3 and leads to products including hydroxy-substituted ON or diketone products. The remaining exocyclic double bond can also be attacked by NO_3 leading to more functionalized products (Fry et al., 2011).

Recently, a class of compounds named highly oxygenated organic molecules (HOM) have been shown to be critical substances in the SOA formation from BVOC oxidation, particularly monoterpenes, featuring high oxidation degree, high O/C ratio and low to extremely low volatility (Ehn et al., 2014; Tröstl et al., 2016; Kirkby et al., 2016; Bianchi et al., 2019). HOM here refers to organic compounds which are formed in the gas phase via autoxidation and contain at least six oxygen atoms (Bianchi et al., 2019). The formation of HOM via autoxidation involves a sequence of multiple intramolecular H-shift and O_2 addition reactions, and results in highly oxygenated peroxy radicals (HOM-RO_2•) (Ehn et al., 2014). Analogous to "traditional" RO_2•, HOM-RO_2• can be involved in similar reactions (Bianchi

https://doi.org/10.5194/acp-2022-85
Preprint. Discussion started: 4 February 2022


Atmospheric Chemistry and Physics Discussions

et al., 2019). The bimolecular reactions of HOM-RO_2• with RO_2•, HO_2• and NO lead to highly oxidized products including carbonyls, hydroperoxides, alcohols, organic nitrates as termination groups, or accretion products, as shown in R1 to R4 (Ehn et al., 2014; Mentel et al., 2015):

$$RO_2• + RO_2• \rightarrow R_HC=O + ROH + O_2 \quad (R1)$$

$$RO_2• + HO_2• \rightarrow ROOH + O_2 \quad (R2)$$

$$RO_2• + NO \rightarrow RONO_2 \quad (R3)$$

$$RO_2• + RO_2• \rightarrow ROOH + O_2 \quad (R4)$$

Unimolecular termination reactions of HOM-RO_2• lead to carbonyls or epoxides (Crounse et al., 2013). In addition, HOM-RO_2• can also be converted to alkoxy radicals (HOM-RO•) through reactions with NO, other RO_2•, or NO_3. If those HOM-RO• undergo an H-migration, they will again form HOM-RO_2 radicals ("alkoxy-peroxy" pathway) (Mentel et al., 2015). HOM-RO• may also fragment leading to small RO_2 radicals (Bianchi et al., 2019).

The clarification of HOM-formation chemistry in limonene + NO_3 system will improve the understanding of the role of HOM for SOA formation as well as the relationship between oxidation products, SOA formation and reaction systems. Donahue et al. (2012) divided atmospheric organics into five categories based on their volatility (saturation concentration, C^*): extremely low volatility organic compounds (ELVOC), low volatility organic compounds (LVOC), semi-volatile organic compounds (SVOC), intermediate volatility organic compounds (IVOC) and volatile organic compounds (VOC). Most HOM are classified as ELVOC or LVOC (Bianchi et al., 2019), and thus HOM can be a substantial source for SOA growth through gas-particle partitioning. Field observations and laboratory simulation experiments have proven the important contribution of HOM in monoterpene + NO_3 SOA (Lee et al., 2016; Faxon et al., 2018). In the SOAS campaign, HOM-ONs (organic nitrates) were identified in both gas and particle phase, including species with the sum formula $C_{10}H_{15,17,19}NO_{4\text{-}11}$ which are formed through the oxidation of monoterpenes by NO_3 (Lee et al., 2016; Massoli et al., 2018). A number of laboratory studies have reported HOM formation by the oxidation of monoterpenes with NO_3. Boyd et al. (2015) observed $C_{10}H_{17}NO_{4/5}$ and $C_{10}H_{15}NO_{5/6}$ in the gas phase in β-pinene + NO_3 experiments and proposed possible formation schemes of these ONs. Nah et al. (2016) further detected 5 and 41 HOM-ONs in the NO_3 oxidation of α-pinene and β-pinene such as $C_{10}H_{15/17/19}NO_{4\text{-}9}$ in the gas- and particle-phase. Claflin and Ziemann (2018) provided formation mechanisms for HOM-ONs via gas-phase and particle-phase reactions in β-pinene + NO_3 experiment. Recently, Shen et al. (2021) found a large number of HOM (>150 species) in the β-pinene + NO_3 reaction. Bell et al. (2021) found that dimer dinitrates ($C_{20}H_{32}N_2O_{8\text{-}13}$) contribute a large portion of SOA from α-pinene + NO_3 and also detected monomer ON such as $C_{10}H_{15}NO_{5\text{-}10}$ and $C_{10}H_{14,16}N_2O_{7\text{-}11}$), although the detailed speciation depends on analytical method to some extent. And the HOM

https://doi.org/10.5194/acp-2022-85
Preprint. Discussion started: 4 February 2022

Atmospheric Chemistry and Physics Discussions

composition in the particle-phase was found to depend on aging time and conditions such as dark versus light (Bell et al., 2021; Wu et al., 2021a). Regarding the reaction of limonene with NO_3, Faxon et al. (2018) reported a series of HOM in the particle phase, including $C_{7\text{-}10}$ monomers with 3-11 oxygen atoms and $C_{11\text{-}20}$ dimers with 5-19 oxygen atoms. However, identification of gas-phase HOM products in the limonene + NO_3 reaction is still lacking and their formation mechanisms remain unclear.

In this study, HOM formation in the NO_3 oxidation of limonene was investigated. We report the identification of gas-phase HOM products, including monomers, dimers and trimers. The formation pathways of dominant products in each category are proposed based on their time profiles in response of multiple additions of limonene in the experiment and on the information in literature. Based on this analysis we estimated HOM yields and discuss the role of HOM in nucleation and SOA growth.

2 Experimental and Methods

2.1 Experimental setup

The limonene + NO_3 experiment was performed in the atmospheric simulation chamber SAPHIR (Simulation of Atmospheric PHotochemistry In a large Reaction chamber) at the Forschungszentrum Jülich, Germany. SAPHIR is a 270 m^3 double-wall cylindrical Teflon chamber with a surface-to-volume ratio of ~1 m^2 m^{-3}. Details of SAPHIR have been described before (Rohrer et al., 2005; Zhao et al., 2015a; Zhao et al., 2015b; Zhao et al., 2018). Detailed experimental procedures can be found in Fig. 1a. Before each experiment, SAPHIR was flushed for about 4 h at a flow rate of 370 m^3 h^{-1} with high-purity synthetic air (purity >99.9999 % O_2 and N_2) in order to clean the chamber. To simulate nighttime conditions for the NO_3 chemistry the chamber roof remained closed throughout the experiment. The experiment was performed under dry conditions (RH <2 %) at a temperature of 302 ± 3 K. No seed aerosols were used in the experiments.

NO_3 radicals were generated via the reaction of ozone with nitrogen dioxide:

$$NO_2 + O_3 \rightarrow NO_3 + O_2 \quad \text{(R5)}$$

$$NO_2 + NO_3 \leftrightarrow N_2O_5 \quad \text{(R6)}$$

Therefore, O_3 and NO_2 were first added to the chamber to form N_2O_5 and NO_3 with mixing ratios of ~2 ppbv and ~0.15 ppbv, respectively. About 20 min later, 6 ppbv of limonene was added to start the organic chemistry. Five more additions of limonene followed with concentrations of about 4 ppbv, 4 ppbv, 3 ppbv, 3 ppbv, and finally 10 ppbv (Fig. 1a), which divided the experiment into six periods (P1 to P6). For period P3 and P5, NO_2 and O_3 were also added to compensate for the loss of NO_3 and N_2O_5 (Fig. 1a). The concentrations of NO_2 and O_3 were maintained

https://doi.org/10.5194/acp-2022-85
Preprint. Discussion started: 4 February 2022


Atmospheric Chemistry and Physics Discussions

around 20 to 70 ppbv throughout the experiment ensuring a major loss of limonene by reaction with NO_3 rather than with O_3 (Fig. S1 in the SI). In the first ten min of reaction (named period P1a hereafter), NO_3 accounted for 86% of the chemical loss of limonene.

2.2 Instrumentation

Gas-phase HOM were detected by a Chemical Ionization time-of-flight Mass Spectrometer (CI-APi-TOF, Aerodyne Research Inc., USA) with a resolution (m/z)/($\Delta m/z$) of ~3800 using $^{15}NO_3^-$ as the reagent ion, which is capable of detecting organic molecules with high oxygen content (Eisele and Tanner, 1993; Jokinen et al., 2012). The mass spectra were analyzed using the software Tofware (Tofwerk/Aerodyne) in Igor Pro (WaveMetrics, Inc.). Peak identification was conducted by a high-resolution analysis. We observed several peaks which were obviously products from the isoprene + NO_3 reaction, such as $C_5H_{10}N_2O_8 \cdot ^{15}NO_3^-$ at m/z 289. Such peaks were present before the limonene oxidation reaction started, suggesting that these compounds preexisted in the chamber. They were likely released from the chamber wall as residue species from an isoprene + NO_3 experiment performed two days before (Zhao et al., 2021) and are not discussed as products from the limonene oxidation in our experiment. (However, we cannot exclude that they were partly generated from fragmentation in the limonene + NO_3 reaction.)

A set of instruments were used to measure other gas-phase species, including VOC, NO_x, O_3, NO_3 and N_2O_5 (Shen et al., 2021). Concentrations of NO_3 and N_2O_5 were measured in-situ using a home-built diode laser-based, cavity ring-down spectrometer similar to the instrument described in the work by Wagner et al. (2011). The concentrations of limonene were measured using a Proton Transfer Reaction Time-of-Flight Mass Spectrometer (PTR-TOF-MS, Ionicon Analytik, Austria). The SOA number concentration, surface concentration and size distribution were detected by an SMPS (TSI DMA3081/TSI CPC3785). Temperature and relative humidity were continuously monitored throughout the experiment.

2.3 Determination of HOM concentration and "primary" HOM yield

HOM concentrations were obtained from the normalized signals to the total signals of the mass spectra (nc, normalized counts) by applying a calibration coefficient (C) of 2.5×10^{10} molecule cm^{-3} nc^{-1}. C was determined using H_2SO_4 as the charging efficiency of HOM and H_2SO_4 are considered to be equal (Ehn et al., 2014; Pullinen et al., 2020; Shen et al., 2021). The details of determination of the calibration coefficient are shown in the supplement S1. A mass-independent transmission efficiency was used according to our previous study, which causes an uncertainty of 14 % (Pullinen et al., 2020). The concentrations of HOM were corrected for a chamber wall loss. As the HOM yield was determined during the first 3 min of the experiment, we considered the wall loss rate to be constant (6×10^{-4} s^{-1}) during this period (Zhao et al., 2018). Sensitivity analysis proved that the HOM yield in this study is not very

https://doi.org/10.5194/acp-2022-85
Preprint. Discussion started: 4 February 2022


Atmospheric Chemistry and Physics Discussions

183 sensitive to the wall loss rate and is changing by 0.24 % and -0.12 % if the wall loss rate is varied by +100 % or -
184 50 %.

185 The HOM yield was calculated as:

186 $$Y = \frac{[HOM]}{[VOC]_r} = \frac{I(HOM) \cdot C}{[N_2O_5]_r} \quad \text{(Eq. 1)}$$

187 where $[HOM]$ is the concentration of HOM, $I(HOM)$ is the total signal intensity of HOM, C the calibration factor,
188 and $[VOC]_r$ and $[N_2O_5]_r$ stand for the concentrations of limonene and N_2O_5 reacted, respectively. We used the
189 reacted concentration of N_2O_5 rather than the measured reacted limonene concentration as a large fraction of limonene
190 was already reacting away during the VOC injection before it was homogeneously mixed in the chamber. During this
191 part of the experiment, the high limonene concentration resulted in a rapid loss of NO_3, such that every NO_3 formed
192 from the decomposition of N_2O_5 reacted with limonene:

193 $$N_2O_5 \rightarrow NO_2 + NO_3 \quad \text{(R7)}$$

194 $$\text{limonene} + NO_3 \rightarrow \text{Products} \quad \text{(R8)}$$

195 The initial NO_3 concentration before the limonene injection was small compared to the time-integrated loss of N_2O_5,
196 and other NO_3 loss processes were negligible right after the limonene injection, so that the observed decrease in the
197 N_2O_5 concentration equals indeed the consumption of limonene.

198 The uncertainty of the HOM yield was estimated to be -55 %/ +117 % based on the combined uncertainties of
199 the HOM-ON peak intensities (~10 %), the limonene concentration (~15 %), the transmission efficiency (-0 %/+14 %)
200 and the calibration factor (-52 %/ +101 %) using error propagation (Zhao et al., 2021). The first 3 min after the
201 injection of limonene were used to calculate the HOM yield, when most of the first-generation oxidation products
202 were produced and negligible particles were yet formed. The HOM yield thus reflects the "primary" HOM yield.

203 **2.4 Determination of HOM condensation on SOA**

204 The SOA mass from the condensation of HOM was calculated to evaluate the role of HOM for the SOA mass growth.
205 Detailed estimation methods are described in the supplement, including the determination of particle wall loss and
206 dilution loss rate (Sect. S2). In brief, the growth rate of SOA through HOM vapor condensation is based on the
207 collision rate of vapor molecules with aerosols in the kinetic regime. The Fuchs-Sutugin approach is applied to
208 describe the correction for transition from the kinetic to the diffusion regime (Fuchs and Sutugin, 1971; Ehn et al.,
209 2014). Based on the volatility of HOM, we considered two scenarios for HOM condensation. In Scenario 1, all HOM
210 were assumed to irreversibly condense on the surface of particles leading to particle mass growth. In Scenario 2, only
211 the irreversible uptake of LVOC and ELVOC compounds were considered to contribute to the SOA growth while

https://doi.org/10.5194/acp-2022-85
Preprint. Discussion started: 4 February 2022

Atmospheric Chemistry and Physics Discussions

IVOC and SVOC were not included. The classification of ELVOC, LVOC, IVOC and SVOC was based on the work by Donahue et al. (2012). The calculation of saturation concentration C^* (in μg/m^3) of each HOM was done based on their molecular compositions using two different parameterizations considering the uncertainties in estimating volatility (Wu et al., 2021b):

1. an updated version of the parametrization of Donahue et al. (2011) by Mohr et al. (2019) (Scenario 2a):

$$log_{10}(C^*) = (25 - n_C) \times 0.475 - (n_O - 3n_N) \times 0.2 - 2\frac{(n_O - 3n_N)n_C}{(n_C + n_O - 3n_N)} \times 0.9 - n_N \times 2.5 \quad \text{(Eq. 2)}$$

where n_C, n_O, n_N and n_H are the number of carbon, oxygen, nitrogen and hydrogen atoms of the compound, respectively.

2. a parameterization based on HOM from α-pinene ozonolysis by Peräkylä et al. (2020) (Scenario 2b):

$$log_{10}(C^*) = n_C \times 0.18 - n_H \times 0.14 - n_O \times 0.38 + n_N \times 0.80 + 3.1 \quad \text{(Eq. 3)}$$

where n_C, n_O, n_N and n_H are the number of carbon, oxygen, nitrogen and hydrogen atoms of the compound, respectively.

2.5 Simulations of the RO_2• loss pathway based on the Master Chemical Mechanism (MCM)

The RO_2• loss pathways were estimated based on MCM simulations (http://mcm.york.ac.uk/). The gas-phase reactions of limonene + NO_3 under dark condition were simulated using iChamber, an open-source program (https://sites.google.com/view/wangsiyuan/models?authuser=0) (Wang and Pratt, 2017). The default chemistry of limonene + NO_3 in the MCM was applied in this study (Saunders et al., 2003). Photolysis reactions were excluded by setting the zenith angle to 90º. Concentrations of O_3, NO_3, NO_2 and N_2O_5 as well as temperature and relative humidity were constrained to the experimental data with a time resolution of 1 min. The chamber dilution rate of 1.5×10^{-5} s^{-1} was applied to all species. The P1 period was simulated using the above conditions and the initial concentrations of limonene were added in the model according to the experimental procedures. The sum of all 140 RO_2• in the limonene subset of MCM v3.3.1 were used in the usual way to estimate the loss rates of RO_2• bimolecular reactions. The reaction rate constants are provided in Table S3, and calculated loss rates are shown in Fig. S2.

In the early stage of each period, RO_2• mainly reacted with RO_2• and NO_3, although in the later stage the reaction with NO_2 also contributed to a significant fraction of RO_2• loss (Fig. S2, showing period P1 as an example). During the period P1a when our peak assignment was based on, the RO_2• loss was dominated by RO_2• + RO_2• and RO_2• + NO_3.

https://doi.org/10.5194/acp-2022-85
Preprint. Discussion started: 4 February 2022

Atmospheric Chemistry and Physics Discussions

3 Results and discussion

3.1 Experiment overview and observed HOM

After each limonene addition, the concentration of limonene rose first and then rapidly declined, while the concentrations of NO_3 and N_2O_5 rapidly decreased due to the fast reaction between limonene and NO_3 and gradually increased when limonene had been consumed (Fig. 1a). About 10 min after the first limonene addition, new particles were formed and quickly grew in size (Fig. 1b). Therefore, we used the first 10 min reaction time (period P1a) to identify gas-phase HOM products, and the whole experiment to examine the contribution of HOM to SOA.

During period P1, HOM were quickly formed. We identified about 280 HOM compounds, including monomers (C_7-C_{10}, ~280-460 Th), dimers (C_{17}-C_{20}, ~490-700 Th), and trimers (C_{26}-C_{30}, ~720-960 Th) (Fig. 2a). Their detailed formulas can be found in Table S1. HOM on the horizontal lines of the Kendrick mass defect plot (O-based) (Fig. 3 and Fig S8, S12) share the same number of C, N and H atoms, with the number of oxygen atoms increasing from left to right. Such HOM compounds are defined as a family. We notice that most monomer peroxy radical families are each related to two monomer closed-shell product families, with one H atom more or one H atom less, which are the expected termination products of RO_2• + RO_2• reactions, or if HO_2• is present, RO_2• + HO_2• termination products. These three related families are defined as a series, with the same number of C and N number, such as $C_{10}H_{15\text{-}17}NO_{6\text{-}14}$. In total, we identified 6 monomer series ($C_{10}H_{15\text{-}17}NO_{6\text{-}14}$, $C_{10}H_{14\text{-}16}N_2O_{9\text{-}15}$, $C_{10}H_{14\text{-}16}O_{7\text{-}12}$, $C_9H_{13\text{-}15}NO_{7\text{-}14}$, $C_8H_{11\text{-}13}NO_{6\text{-}13}$ and $C_7H_{9\text{-}11}NO_{7\text{-}11}$) and 1 monomer family ($C_{10}H_{17}N_3O_{12\text{-}16}$), 11 dimer families ($C_{20}H_{31}NO_{10\text{-}15}$, $C_{20}H_{33}NO_{12\text{-}16}$, $C_{20}H_{32}N_2O_{9\text{-}20}$, $C_{20}H_{31}N_3O_{14\text{-}20}$, $C_{20}H_{33}N_3O_{12\text{-}20}$, $C_{20}H_{34}N_4O_{15\text{-}20}$, $C_{20}H_{32}O_{13\text{-}16}$, $C_{19}H_{29}NO_{10\text{-}13}$, $C_{19}H_{31}NO_{10\text{-}15}$, $C_{19}H_{30}N_2O_{10\text{-}18}$ and $C_{19}H_{31}N_3O_{15\text{-}19}$), and 3 trimer families ($C_{30}H_{47}N_3O_{18\text{-}24}$, $C_{30}H_{48}N_4O_{16\text{-}24}$ and $C_{29}H_{46}N_4O_{19\text{-}24}$). Compounds containing at least one nitrogen atom accounted for more than 90 % of the identified HOM products while the remaining fraction were non-nitrated products. We assume that compounds containing nitrogen atoms are organic nitrates, because other N-containing species such as amines or nitro compounds are very unlikely formed from the reaction of limonene with NO_3. Organic nitrates formed in this study could be alkylnitrates or peroxynitrates via the reaction of RO_2• with NO_2.

During period P1a, in the absence of particles, both HOM monomers and oligomers were observed, including monomers (47 %), dimers (47 %) and trimers (6 %) (Fig. 2a). Concentrations of gas-phase dimers and trimers decreased evidently after particle formation (Fig. 2b, 5, 6), indicating a fast gas-particle condensation and strong tendency of oligomers to condense on particles.

https://doi.org/10.5194/acp-2022-85
Preprint. Discussion started: 4 February 2022

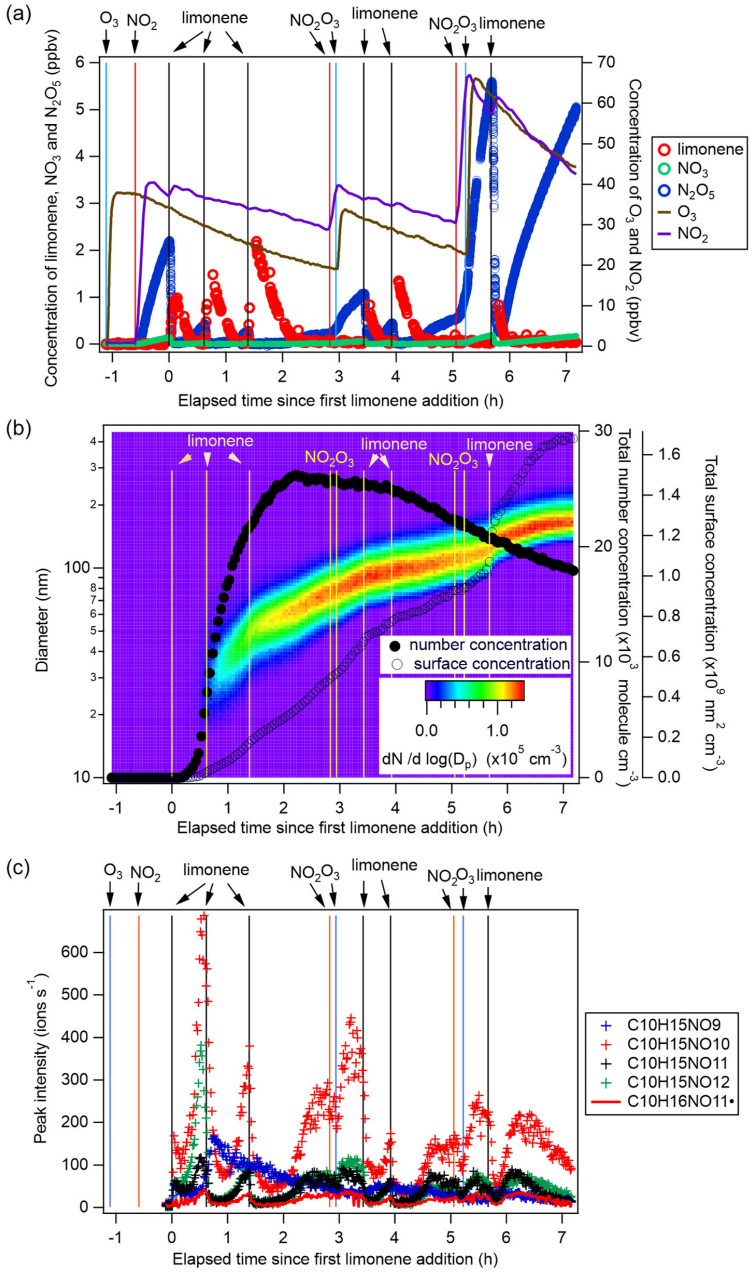

Figure 1. (a) Time series of the concentrations of limonene, NO_3, N_2O_5 (left panel), as well as O_3 and NO_2 (right panel). (b) Total particle concentration and its size distribution during the whole period of experiment detected by SMPS. The solid and hollow black circles refer to total number concentration and total surface concentration, respectively. Colors represent particle number concentration distribution based on $\log(D_p)$. (c) Time series of peak

https://doi.org/10.5194/acp-2022-85
Preprint. Discussion started: 4 February 2022

Atmospheric Chemistry and Physics Discussions

intensity of typical products of the $C_{10}H_{15}NO_x$ family and $C_{10}H_{16}NO_{11}$• as a representative of the $C_{10}H_{16}NO_x$• family. Vertical lines indicate the time of O_3 and NO_2 addition, as well as six limonene injections.

Based on their typical time series, products can be classified as first-generation or second-generation products (Fig. 1c). Generally, the concentrations of first-generation products, which result from the direct reaction of limonene with NO_3, are expected to quickly increase after the limonene addition, followed by a steady decline due to wall loss or chemical reactions. Concentrations of typical second-generation products, which result from further reactions of first-generation products, are expected to show a gradually increasing concentration pattern after a limonene addition and reach their maximum contribution later than first-generation products. These general expectations are modified in our case, since the particle concentration increased in our experiment (Fig. 1b) and the condensational sink of HOM products became stronger over time. Thus, an increase in concentration suggests an overcome of the increasing condensational sink by increasing production with time, i.e. from second-generation pathways.

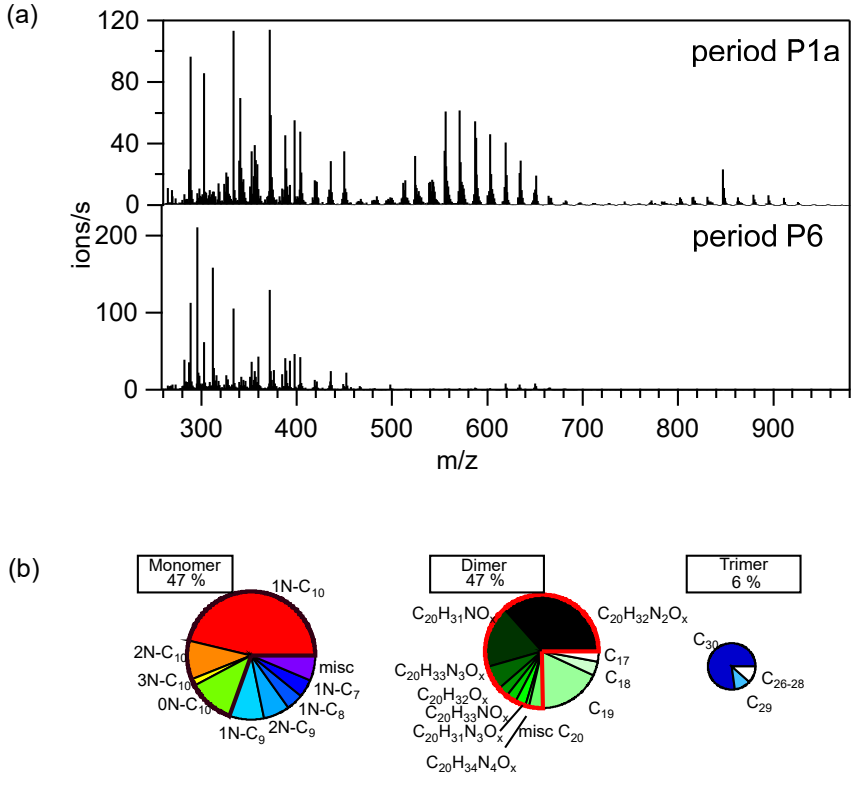

Figure 2. (a) Average mass spectra of the first 10 min reaction time after the first addition of limonene (period P1a,

https://doi.org/10.5194/acp-2022-85
Preprint. Discussion started: 4 February 2022

Atmospheric Chemistry and Physics Discussions

upper panel) and the last limonene addition period till particles reached maximum mass concentration (period P6, lower panel). (b) Pie charts (from left to right: rainbow, green, and blue colors) representing the relative contributions of identified series/families to HOM monomers, dimers, and trimers, respectively, during the P1a period. The area of each pie is in proportion to their concentrations during the P1a period.

3.2 Monomers and their formation pathways

3.2.1 Overview of HOM monomers

A number of HOM monomer families were detected with an increasing oxygenation pattern at 16 Th intervals (Fig. 3). During period P1a, the most abundant HOM monomers are C_{10} compounds (64 %), such as peroxy radicals $C_{10}H_{16}NO_x$• and closed-shell products $C_{10}H_{15}NO_x$ and $C_{10}H_{17}NO_x$, which are carbonyl compounds and hydroxyl or hydroperoxy compounds from the termination reactions of $C_{10}H_{16}NO_x$•, respectively. According to the nitrogen atoms contained, C_{10}-HOM monomers can be classified into 1N-, 2N, 3N-monomers and monomers without nitrogen atoms. While 1N-C_{10} HOM monomers were likely formed by direct NO_3 addition to limonene, C_{10}-HOM monomers containing multiple N atoms were likely formed via multiple reaction steps. Besides C_{10} HOM monomers, $C_{6\text{-}9}$ HOM monomers were also observed. These $C_{6\text{-}10}$ families are discussed below in the order of their contributions to HOM monomers.

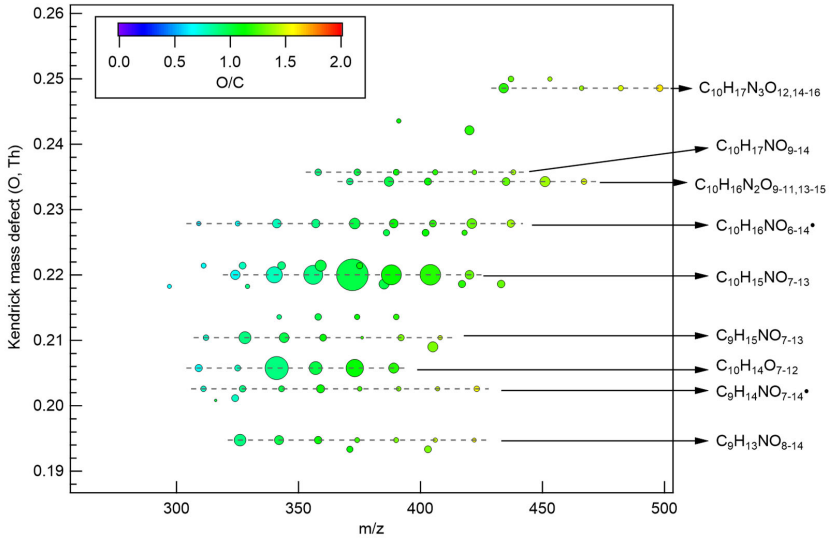

Figure 3. Kendrick mass defect plot (O-atom-based) of major monomer products. The area of the circles is proportional to the average intensity of each compound during the P1a period with the largest circle representing

https://doi.org/10.5194/acp-2022-85
Preprint. Discussion started: 4 February 2022


Atmospheric Chemistry and Physics Discussions

$C_{10}H_{15}NO_{10}$. The color denotes O/C ratios. Dashed lines indicate major product families. For clarity, the reagent ions $^{15}NO_3^-$ is omitted from molecular formula.

3.2.2 1N-C_{10} monomers

Among C_{10} HOM monomers, the 1N-C_{10} families were most abundant and included stable closed-shell products $C_{10}H_{15}NO_x$ (x=7-13) and $C_{10}H_{17}NO_x$ (x=9-14) and peroxy radicals $C_{10}H_{16}NO_x$• (x=6-14). The concentration of $C_{10}H_{16}NO_{11}$• increased in the later phase of each limonene addition period (Fig. 1c), showing mostly a time profile of a second-generation product, similar as most of the other radicals in the $C_{10}H_{16}NO_x$• family (Fig. S3). However, the time series of $C_{10}H_{15}NO_x$ compounds showed an overlaying pattern of first- and second-generation products dominated by a second-generation time profile with the exception of $C_{10}H_{15}NO_9$ (Fig. 1c). Given that RO_2• are chemically active, it is likely that $C_{10}H_{16}NO_x$• radicals converted immediately after their formation, so that their concentrations did not exhibit a first-generation time profile. At this time, we do not have a reasonable explanation for the trend of $C_{10}H_{15}NO_9$.

Since the $C_{10}H_{15}NO_x$ family showed an overlaying pattern of the first-generation and second-generation products, they likely contained multiple isobaric substances produced through different pathways. Based on the literature, possible formation pathways of these products were tentatively proposed (Seinfeld and Pandis, 2006; Vereecken and Peeters, 2010; Mentel et al., 2015; Vereecken and Nozière, 2020). As an example of the pathways to form first-generation products, $C_{10}H_{16}NO_{2x-1}$• (with an odd number of oxygen atom) and their corresponding termination products can be formed via autoxidation of the first peroxy radical $C_{10}H_{16}NO_5$• (R1OO), showing $C_{10}H_{16}NO_9$• (R3OO) as an example (Scheme 1a, first-generation products). $C_{10}H_{16}NO_{2x}$• (with an even number of oxygen atom) can be formed via alkoxy-peroxy channels. For example, the ring-opening of the alkoxy radical $C_{10}H_{16}NO_4$• (R1O), which was formed via the reaction of $C_{10}H_{16}NO_5$• (R1OO) with another RO_2 radical or NO_3 (Scheme 1a, first-generation products). Ring-opening of R1O lead to $C_{10}H_{16}NO_6$• (R4OO), which can undergo autoxidation forming $C_{10}H_{16}NO_{2x}$•. In addition, the alkoxy radical $C_{10}H_{16}NO_4$• (R1O) is susceptible to ring-opening reactions (Novelli et al., 2021), which can lead to a first-generation stable product 3-isopropenyl-6-oxoheptanal (endolim, TP1) after C-C bond cleavage followed by the elimination of a NO_2 fragment (Scheme 1b, second-generation products). Endolim (TP1) has been detected as a major product in previous limonene + NO_3 studies (Hallquist et al., 1999; Spittler et al., 2006).

As an example of second-generation chemistry, the remaining double bond of endolim could react with NO_3 to form RO_2•, followed by the autoxidation to form second-generation $C_{10}H_{16}NO_x$• (with odd number of oxygen atoms).

https://doi.org/10.5194/acp-2022-85
Preprint. Discussion started: 4 February 2022

Atmospheric Chemistry and Physics Discussions

338 Similar to first-generation pathways, second-generation $C_{10}H_{16}NO_x$• with even number of oxygen atoms can be
339 formed via alkoxy-peroxy channel. From the time profile of $C_{10}H_{15}NO_x$, the second-generation pathway (Scheme 1b)
340 was expected to play a more important role, in agreement with the theoretical result by Kurtén et al. (2017), in which
341 the two bond-cleavage pathways of limonene-derived RO• radical were considered. It is worth mentioning that the
342 reaction products of limonene with O_3 may also react with NO_3, forming $C_{10}H_{16}NO_x$• (Scheme S1). However, as
343 shown above, this was a minor pathway in our experiment (Sect. 2.1). We would like to note that to simplify the
344 scheme, only the reaction of NO_3 with the endocyclic double bond is presented, since this reaction is faster than that
345 with the exocyclic double bond (Jiang et al., 2009; Fry et al., 2011).

346 $C_{10}H_{16}NO_x$• with both even and odd number of oxygen atoms as well as their termination products had
347 comparable abundance, which suggests that the alkoxy-peroxy pathway was important for RO_2• formation in this
348 reaction. This finding is analogous to the findings in the reaction of a number of alkenes with O_3 and in the reaction
349 of isoprene and β-pinene with NO_3 (Mentel et al., 2015; Zhao et al., 2021; Shen et al., 2021).

350

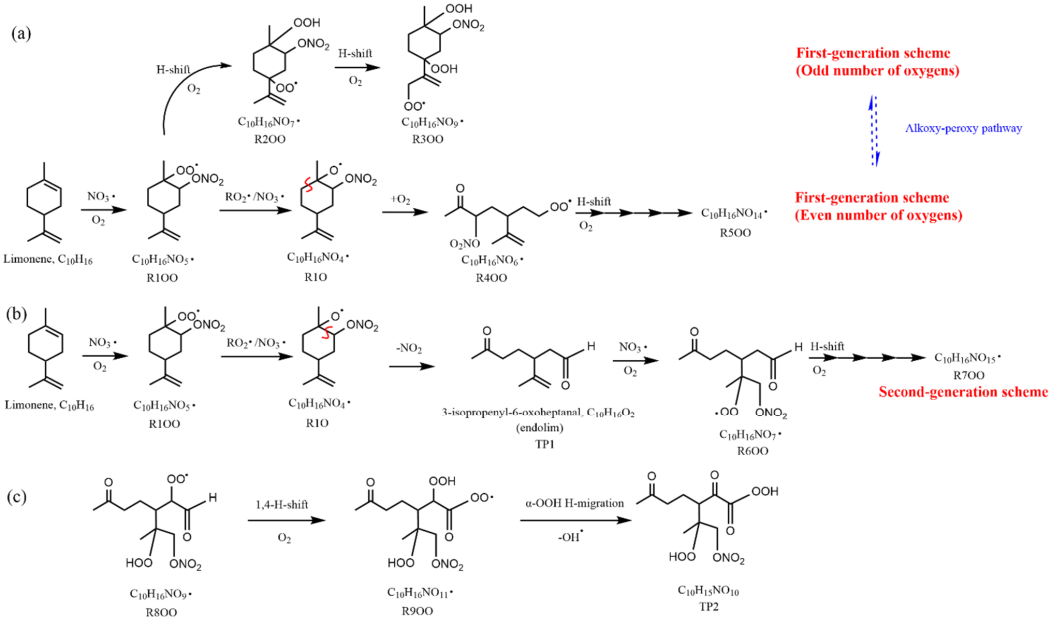

351

352 Scheme 1. Illustrative scheme for HOM formation in the limonene + NO_3 reaction. (a) Example formation pathways
353 leading to first-generation 1N-C_{10} HOM-RO_2 radicals ($C_{10}H_{16}NO_x$• with even or odd numbers of O-atoms). (b)
354 Second-generation scheme involving the formation of endolim. (c) Scheme of intramolecular termination of RO_2•
355 radicals forming carbonyl products taking the $C_{10}H_{16}NO_9$• radical as an example. Note that the depicted reactions

https://doi.org/10.5194/acp-2022-85
Preprint. Discussion started: 4 February 2022

Atmospheric Chemistry and Physics Discussions

may not be the dominant pathways.

Among 1N-C_{10} monomers, concentrations of carbonyl compounds were much higher than the sum of hydroxy- and hydroperoxy-substituted compounds (Table 1). This finding is likely attributed to unimolecular termination reactions of RO_2•. The importance of unimolecular termination reactions of HOM-RO_2• and the resulting high ratio of carbonyl compounds to hydroxyl/hydroperoxyl compounds has also been found in the reaction system of β-pinene + NO_3 (Shen et al., 2021). This high ratio is also consistent with findings in the ozonolysis of alkenes (Mentel et al., 2015), where unimolecular termination reactions were also proposed to be the likely explanation (Crounse et al., 2013; Rissanen et al., 2014). Our result thus further emphasizes that unimolecular termination reactions of RO_2 radicals are important pathways in the formation of HOM monomers derived from the reactions of monoterpenes with NO_3 (Shen et al., 2021). Scheme 1c shows this intramolecular termination process using a $C_{10}H_{16}NO_9$• radical as an example. $C_{10}H_{16}NO_9$• undergoes a 1,4-H-shift and O_2 addition to form a $C_{10}H_{16}NO_{11}$• radical. The $C_{10}H_{16}NO_{11}$• radical further undergoes an H-shift of the α-OOH H-atom, which produces a carbonyl closed-shell product as well as an OH• radical.

For 1N-C_{10} HOM monomers, the products detected in this study generally agree with previous laboratory and field studies on the reaction of limonene and other monoterpenes. Faxon et al. (2018) also observed $C_{10}H_{15}NO_x$ as the most prevalent products in the particle phase from limonene + NO_3. In the SOAS campaign, both $C_{10}H_{15}NO_x$ and $C_{10}H_{17}NO_x$ products were detected and were believed to be products of nighttime chemistry (Lee et al., 2016). The high abundance of 1N-C_{10} HOM monomers is consistent with the finding that $C_{10}H_{15}NO_x$ and $C_{10}H_{17}NO_x$ dominate the chemical composition of SOA formed via NO_3 oxidation of α-pinene and β-pinene, as shown in previous chamber studies (Takeuchi and Ng, 2019).

Table 1. Observed $C_{10}H_{16}NO_x$• radicals (m) and their termination products, including carbonyl compounds (m-17), hydroxyl compounds (m-15), and hydroperoxy compounds (m+1). Their concentrations during period P1a are normalized to that of $C_{10}H_{15}NO_{10}$, which had the highest concentration among the family series of 1N-C_{10} monomers. Their relative intensities during the P1a period are shown in the second line of each cell.

Peroxy radical **m**	**Carbonyl** **m-17**	**Hydroxy** **m-15**	**Hydroperoxy** **m+1**
$C_{10}H_{16}NO_6$• 1.5 %			

https://doi.org/10.5194/acp-2022-85
Preprint. Discussion started: 4 February 2022

Atmospheric Chemistry and Physics Discussions

$C_{10}H_{16}NO_7$• 2.0 %			
$C_{10}H_{16}NO_8$• 6.7 %	$C_{10}H_{15}NO_7$ 8.0 %		
$C_{10}H_{16}NO_9$• 6.0 %	$C_{10}H_{15}NO_8$ 25.2 %		$C_{10}H_{17}NO_9$ 3.7 %
$C_{10}H_{16}NO_{10}$• 10.2 %	$C_{10}H_{15}NO_9$ 34.6 %	$C_{10}H_{17}NO_9$ 3.7 %	$C_{10}H_{17}NO_{10}$ 3.6 %
$C_{10}H_{16}NO_{11}$• 6.6 %	$C_{10}H_{15}NO_{10}$ 100.0 %	$C_{10}H_{17}NO_{10}$ 3.6 %	$C_{10}H_{17}NO_{11}$ 3.0 %
$C_{10}H_{16}NO_{12}$• 4.1 %	$C_{10}H_{15}NO_{11}$ 39.0 %	$C_{10}H_{17}NO_{11}$ 3.0 %	$C_{10}H_{17}NO_{12}$ 2.3 %
	$C_{10}H_{15}NO_{12}$ 41.2 %	$C_{10}H_{17}NO_{12}$ 2.3 %	$C_{10}H_{17}NO_{13}$ 1.5 %
$C_{10}H_{16}NO_{14}$• 4.7 %	$C_{10}H_{15}NO_{13}$ 6.7 %	$C_{10}H_{17}NO_{13}$ 1.5 %	$C_{10}H_{17}NO_{14}$ 1.8 %
		$C_{10}H_{17}NO_{14}$ 1.8 %	

3.2.3 2N and 3N-C_{10} monomers

C_{10} monomers with 2 and 3 nitrogen atoms accounted for 27 % and 1 % of HOM monomers, respectively. They were likely formed via the reaction of a second attack of NO_3 to the first-generation products with the remaining double bond from limonene. The 1N-C_{10} closed-shell products formed via the reactions shown in Scheme 1a should contain a remaining C=C double bond. Typical 2N- and 3N- HOM showed a second-generation time profile (Fig. 4). For clarity, only periods P1 to P3 are shown. This time profile is consistent with the pathways with multiple NO_3 attacks. Scheme 2 shows possible formation pathways of 2N- and 3N-C_{10} monomers. 2N-C_{10} HOM were likely to be formed from NO_3 oxidation of 1N-C_{10} monomers ($C_{10}H_{15}NO_x$ and $C_{10}H_{17}NO_x$), resulting in $C_{10}H_{15}N_2O_x$• and $C_{10}H_{17}N_2O_x$• (Scheme 2a, 2b). While $C_{10}H_{15}N_2O_x$• (x=9-12) were observed, $C_{10}H_{17}N_2O_x$• could not be uniquely identified because the peaks of the $C_{10}H_{17}N_2O_x$• and $C_{10}H_{15}NO_x$ families are too close in the mass spectra to be separated based on the resolution of our mass spectrometer. 3N-C_{10} monomers, $C_{10}H_{17}N_3O_x$, were expected to be formed via two steps of NO_3 oxidation to the double bonds and an addition of NO_2 to RO_2 radical, leading to a peroxynitrate or peroxyacylnitrate. NO_2 addition reactions may also contribute to the formation of 2N-C_{10} monomers. The addition of NO_2 to RO_2 radicals could occur either before (Scheme 2d) or after (Scheme 2c) the second NO_3 attack.

https://doi.org/10.5194/acp-2022-85
Preprint. Discussion started: 4 February 2022

Atmospheric Chemistry and Physics Discussions

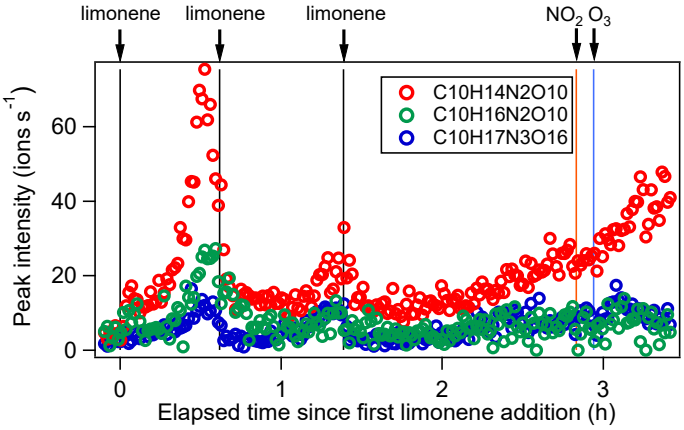

398

399 Figure 4. Time series of peak intensity of several monomers $C_{10}H_{14}N_2O_{10}$, $C_{10}H_{16}N_2O_{10}$ and $C_{10}H_{17}N_3O_{16}$ as the
400 representatives of multiple N monomers during the periods P1-P3.

401

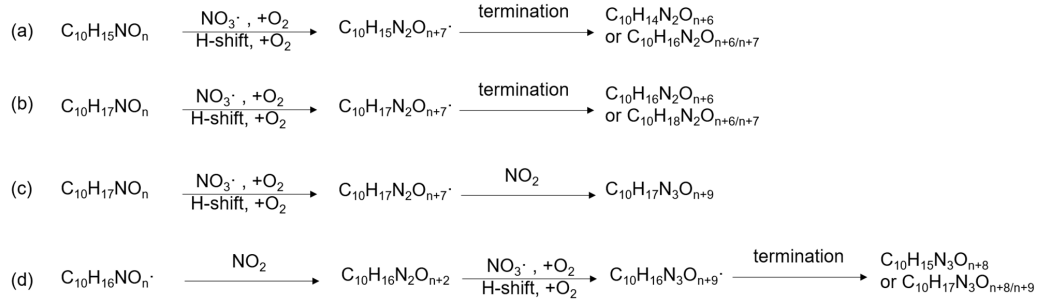

402

403 Scheme 2. Possible formation pathways of C_{10}-monomers containing 2 nitrogen atoms (a, b) and 3 nitrogen atoms
404 (c, d). Termination denotes reactions of RO_2• with other RO_2• or HO_2•, or unimolecular reactions, leading to closed-
405 shell products.

406 **3.2.4 Formation pathways of C_{10} monomers without N-atoms and monomers with less than 10 C-atoms**

407 Besides C_{10} products containing nitrogen atoms, HOM monomers without nitrogen atoms were also identified.
408 Among these products, $C_{10}H_{14}O_x$ (x=7-12) were the most prevalent family, which were also detected in limonene
409 ozonolysis (Jokinen et al., 2015). The $C_{10}H_{14}O_x$ family showed a time series typical of first-generation products (Fig.
410 S4). $C_{10}H_{14}O_x$ and $C_{10}H_{16}O_x$ could be formed from limonene + NO_3 with $C_{10}H_{16}NO_x$• terminating their autoxidation
411 by migration of the α-NO_3 H-atom, eliminating an NO_2 fragment (Scheme S2) (Novelli et al., 2021). Alternatively,
412 these products could be formed via the reaction of O_3 with limonene (Scheme S2). In either way, $C_{10}H_{14}O_x$ and

https://doi.org/10.5194/acp-2022-85
Preprint. Discussion started: 4 February 2022


Atmospheric Chemistry and Physics Discussions

$C_{10}H_{16}O_x$ were formed via first-generation pathways.

We also observed monomers with carbon atom number less than 10. During the P1a period, C_9 monomer families were the most abundant contributors to C<10 HOM monomers, followed by C_8 families. The majority of C_9 monomers were $C_9H_{15}NO_x$ (x=7-13) and $C_9H_{13}NO_x$ (x=8-14). The loss of one carbon atom may follow the mechanism shown in Scheme S3 (Fry et al., 2011; Bianchi et al., 2019). The major product family in C_8 monomers is $C_8H_{11}NO_x$ (x=6, 7, 9-13). While during period P1a $C_8H_{11}NO_x$ compounds could be hardly observed, their concentrations increased considerably in the later periods (Fig. S6). The gas-phase concentration of $C_8H_{11}NO_7$ was even the highest among all compounds in later periods (highest intensity signal in Fig. 2b). This is partly attributed to the relatively high volatility of C8 compounds compared with C10 HOM species and accretion products, which tend to condense on particles. The major family in C_7 monomers, $C_7H_9NO_x$ (x=6-13), showed a time series pattern similar to $C_8H_{11}NO_x$ compounds (Fig. S7). Such a time profile indicates that C_7 and C_8 products were likely a result of multi-generation gas-phase reactions.

3.3 Dimers and their formation

Among dimers, C_{20} products were the most abundant, followed by C_{19} products. Among C_{20} and C_{19} dimers, the most prevalent families included $C_{20}H_{32}N_2O_x$ (x=9-20), $C_{20}H_{33}N_3O_x$ (x=12-20), $C_{20}H_{31}NO_x$ (x=10-15), $C_{20}H_{31}N_3O_x$ (x=14-20), $C_{20}H_{34}N_4O_x$ (x=15-20), and $C_{19}H_{30}N_2O_x$ (x=10-18) (Fig. S8). The O/C ratio of dimers did not exceed one, while that of monomers was as high as two. This could be due to oxygen atom loss and participation of less oxygenated RO_2• in the dimer formation as discussed below. Time series of dimers also showed different patterns compared to monomers. For example, compounds of the $C_{20}H_{32}N_2O_x$ family only reached a considerable peak intensity in period P1 and decreased rapidly, and the signal intensity in periods P2 to P6 were low (Fig. 5). Other dimers showed similar patterns (Fig. S9-11). The time when signals of dimers dropped substantially matched the time of new particle formation (NPF) and the onset of particle growth, indicating that dimers were likely to contribute to early growth of particles. Such a behavior is expected since dimers have a much lower volatility than monomers. This observation is consistent with the laboratory study by Faxon et al. (2018) that found a significant fraction of HOM dimer derived from limonene + NO_3 in the particle phase.

https://doi.org/10.5194/acp-2022-85
Preprint. Discussion started: 4 February 2022

Atmospheric Chemistry and Physics Discussions

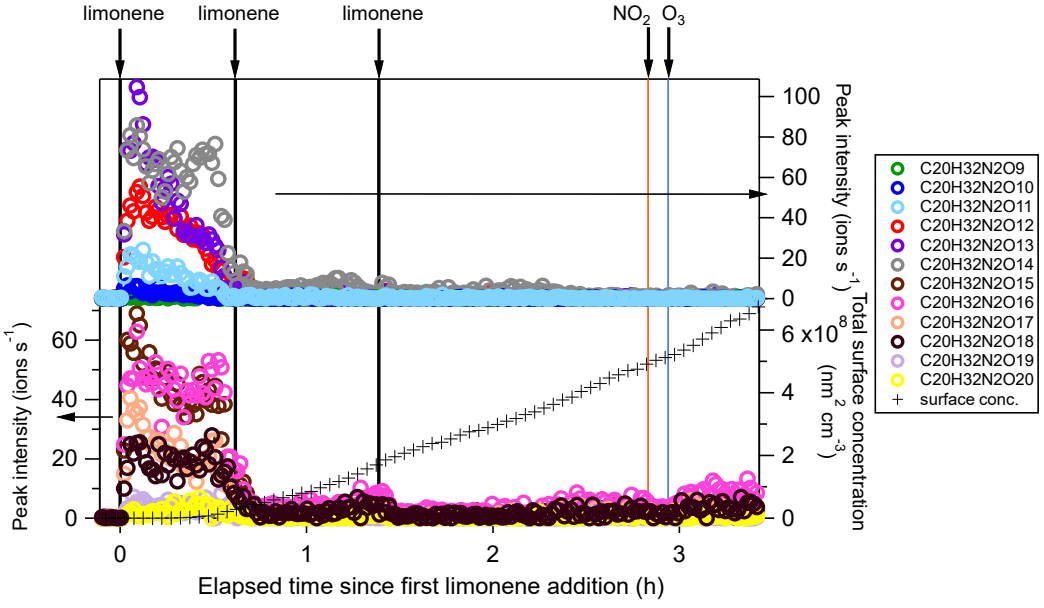

Figure 5. Time series of peak intensity of the $C_{20}H_{32}N_2O_x$ family compounds during the periods P1 to P3. The cross markers (lower right y-axis) indicate total particle surface concentration.

In general, $C_{20}H_{32}N_2O_x$ showed an overlaying time profile of first- and second-generation products (Fig. 5). $C_{20}H_{32}N_2O_x$ were likely formed via the accretion reaction between two monomer RO_2• ($C_{10}H_{16}NO_x$•):

$$C_{10}H_{16}NO_{x1}\bullet + C_{10}H_{16}NO_{x2}\bullet \rightarrow C_{20}H_{32}N_2O_{x1+x2-2} + O_2 \quad \text{(R9)}$$

Since $C_{10}H_{16}NO_x$• can be first- or second-generation products, the resulting dimers $C_{20}H_{32}N_2O_x$ can also be first- or second-generation products. Time series showed that $C_{20}H_{32}N_2O_x$ with less O number presented more of a first-generation product time profile (Fig. 5). The relative contribution of second-generation formation tended to increase with oxygen number.

We compared the observed dimer formula with those expected based on accretion reactions of HOM-RO_2•. X in the $C_{20}H_{32}N_2O_x$ observed was ≥ 9; however, according to the accretion mechanism and the observed $C_{10}H_{16}NO_x$• (x ≥ 6), x in $C_{20}H_{32}N_2O_x$ should be ≥ 10 (6+6-2=10). Moreover, as the most abundant RO_2• within the $C_{10}H_{16}NO_x$• family was $C_{10}H_{16}NO_{10}$• (Table 1), the most abundant $C_{20}H_{32}N_2O_x$ was expected to have an oxygen number of 18 according to the accretion reaction mechanism. This contradicted the fact that the most abundant molecule among the $C_{20}H_{32}N_2O_x$ family was $C_{20}H_{32}N_2O_{13}$. The findings above could only be explained by the participation of less oxygenated RO_2• such as $C_{10}H_{16}NO_{5,6}$• in the accretion reaction (Berndt et al., 2018a; Berndt et al., 2018b; Mcfiggans

https://doi.org/10.5194/acp-2022-85
Preprint. Discussion started: 4 February 2022

Atmospheric Chemistry and Physics Discussions

et al., 2019; Pullinen et al., 2020). $C_{10}H_{16}NO_5$• was not detected in by our CI-APi-TOF, which is attributed to the lower detection sensitivity of molecules with O number ≤ 5 in the NO_3^--CIMS (Riva et al., 2019). $C_{10}H_{16}NO_5$• is the first RO_2 radical formed in the limonene + NO_3 reaction (Scheme 1a). If we assume that the abundance of $C_{10}H_{16}NO_5$• was high, and considering that the concentration of $C_{10}H_{16}NO_{10}$• was the highest in the $C_{10}H_{16}NO_x$• family, their accretion reaction (R10) could form $C_{20}H_{32}N_2O_{13}$ and justify that $C_{20}H_{32}N_2O_{13}$ was the most abundant C_{20} dimer product:

$$C_{10}H_{16}NO_5• + C_{10}H_{16}NO_{10}• \rightarrow C_{20}H_{32}N_2O_{13} + O_2 \quad \text{(R10)}$$

Time series of dimers with unequal numbers of N atoms were different, indicating different formation pathways. For example, the $C_{20}H_{31}NO_x$ family were mainly first-generation products (Fig. S9), which may be formed via the following reaction:

$$C_{10}H_{16}NO_{x1}• + C_{10}H_{15}O_{x2}• \rightarrow C_{20}H_{31}NO_{x1+x2-2} + O_2 \quad \text{(R11)}$$

$C_{10}H_{15}O_x$• were first-generation radicals (Sect. 3.2.4), while $C_{10}H_{16}NO_x$• were mainly second-generation radicals. $C_{10}H_{16}NO_x$• could also be formed via first-generation pathway as discussed above (Scheme 1a), but that was not apparent by the time profile, suggesting a fast termination of first-generation $C_{10}H_{16}NO_x$• radicals. Reaction R11 could be one of the termination pathways of first-generation $C_{10}H_{16}NO_x$• based on the first-generation time profile of $C_{20}H_{31}NO_x$. In the study by Faxon et al. (2018), the formation of 1N-C_{20} dimers was explained by a mechanism involving two 1N-RO_2 radicals which produced HNO_3 as a by-product. However, C_{10} RO_2 radicals without nitrogen atoms were identified in our study, which provided a direct formation pathway of 1N-C_{20} dimers through R11.

On the other hand, $C_{20}H_{33}N_3O_x$ and $C_{20}H_{34}N_4O_x$ were mainly second-generation products (Fig. S10, 11). $C_{20}H_{33}N_3O_x$ and $C_{20}H_{34}N_4O_x$ were likely to be formed via NO_3 oxidation of dimers containing less nitrogen atoms, and were thus second-generation products. The related radicals were also detected, such as $C_{20}H_{32}N_3O_x$• (x=16-19) and $C_{20}H_{31}N_2O_x$• (x=13-16). Possible formation pathways of dominant oligomer families are displayed in Table 2.

Table 2. Major dimer and trimer families and their possible formation pathways.

Dimer/Trimer family	Possible formation pathways
$C_{20}H_{32}N_2O_x$	$C_{10}H_{16}NO_x$• + $C_{10}H_{16}NO_x$•
$C_{20}H_{33}N_3O_x$ / $C_{20}H_{31}N_3O_x$	$C_{20}H_{32}N_2O_x$ + NO_3 + HO_2•/RO_2•
$C_{20}H_{31}NO_x$	$C_{10}H_{16}NO_x$• + $C_{10}H_{15}O_x$•
$C_{20}H_{33}NO_x$	Unknown

https://doi.org/10.5194/acp-2022-85
Preprint. Discussion started: 4 February 2022

Atmospheric Chemistry and Physics Discussions

$C_{20}H_{34}N_4O_x$	Unknown
$C_{19}H_{30}N_2O_x$	$C_{10}H_{16}NO_x$• + $C_9H_{14}NO_x$•
$C_{19}H_{31}N_3O_x$	$C_{19}H_{30}N_2O_x$ + NO_3 + HO_2•/RO_2•
$C_{19}H_{29}NO_x$	$C_9H_{14}NO_x$• + $C_{10}H_{15}O_x$•
$C_{19}H_{31}NO_x$	Unknown
$C_{30}H_{48}N_4O_x$	$C_{20}H_{32}N_3O_x$• + $C_{10}H_{16}NO_x$•
$C_{30}H_{47}N_3O_x$	$C_{20}H_{31}N_2O_x$• + $C_{10}H_{16}NO_x$•

3.4 Trimers and their formation

Trimers were dominated by C_{30} compounds (Fig. S12). To the best of our knowledge, this is the first study that identified gas-phase trimers in the limonene + NO_3 reaction. The O/C ratio of trimers were lower than that of monomers and dimers, suggesting possible multiple accretion reactions in their formation pathways, which lose 2 oxygen atoms in each reaction. As each accretion reaction terminates peroxy radicals, the observation of trimers also implies that some dimers could further react with NO_3. The most prevalent product families were $C_{30}H_{48}N_4O_x$ (x=16-24) and $C_{30}H_{47}N_3O_x$ (x=18,19,21,23,24), which were likely formed via the most abundant monomer RO_2• radicals - $C_{10}H_{16}NO_x$• and the most abundant dimer RO_2 radicals - $C_{20}H_{32}N_3O_x$• and $C_{20}H_{31}N_2O_x$•. Trimers from other monoterpenes + NO_3 have been observed in previous laboratory studies. For example, $C_{30}H_{48}N_4O_{16}$ and $C_{30}H_{47}N_3O_{16}$ were observed in the mass spectra of α-pinene + NO_3 SOA by Wu et al. (2021a), and $C_{30}H_{47}N_3O_{13}$ was identified in β-pinene + NO_3 SOA by Claflin and Ziemann (2018).

Similar to their precursors $C_{20}H_{32}N_2O_x$, $C_{30}H_{48}N_4O_x$ showed negligible signal except in period P1, and presented an overlaying time profile of first- and second-generation product pattern (Fig. 6). For comparison, gas-phase trimer products were not observed in the β-pinene + NO_3 reaction (Shen et al., 2021), and the trimers observed in SOA from β-pinene + NO_3 were likely formed via particle phase reactions (Claflin and Ziemann, 2018). An efficient gas-phase trimer production via subsequent accretion reactions between peroxy radicals requires that the precursor dimer has high enough reactivity to create a dimer RO_2•, e.g. via NO_3 reaction to a double bond. This suggests that the VOC containing at least two double bonds are likely more favorable to form trimers, which is consistent with our previous findings that trimers were formed in the NO_3 reaction with isoprene which also contains two double bonds (Zhao et al., 2021) while they were not observed in the reaction of NO_3 with β-pinene which contains only one double bond (Shen et al., 2021).

https://doi.org/10.5194/acp-2022-85
Preprint. Discussion started: 4 February 2022

Atmospheric Chemistry and Physics Discussions

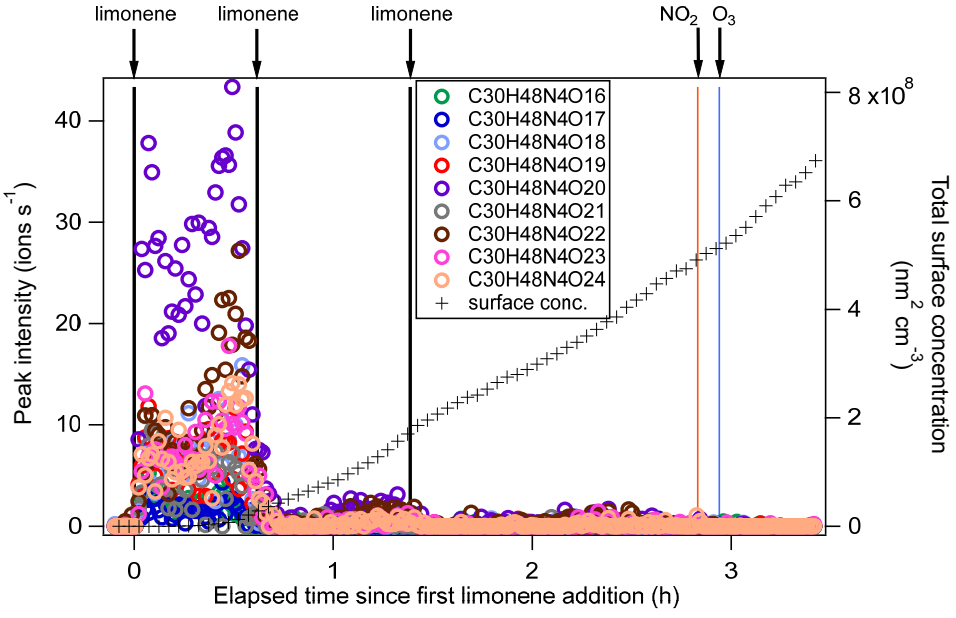

Figure 6. Time series of peak intensity of the $C_{30}H_{48}N_4O_x$ family compounds during the periods P1 to P3. The cross markers (right y-axis) indicate total particle surface concentration.

3.5 "Primary" incremental HOM yields

We chose period P1 for the calculation of HOM yields in order to minimize the influence of the condensational sink on HOM concentration. However, both first-generation and second-generation products existed in this period, as discussed in Sect. 3.2 through 3.4 and supported by the time-behavior of the total HOM concentration (Fig. S13). Period P1 can be roughly divided into three phases based on the trend of HOM concentration. Shortly after the limonene injection, large quantities of HOM were produced (first-production phase) followed by a steady intermediate phase when HOM concentrations stopped increasing. After the intermediate phase, HOM concentrations began to increase again (second-production phase). The first-production phase overlapped with the time span where limonene, NO_3 and N_2O_5 concentrations decreased, implying the dominance of first-generation HOM production process. During the second production period, wall loss was compensated by second-generation HOM formation, leading to another rise of the total HOM concentrations. Therefore, we use the first-production phase to estimate primary HOM production, determined over the first 3 min of the experiment. The calculated "primary" HOM molar yield is 1.5 $\%^{+1.7\ \%}_{-0.7\ \%}$. This value is significantly lower than the HOM yield of 5 to 17 % in earlier limonene ozonolysis experiments (Ehn et al., 2014; Jokinen et al., 2015; Pagonis et al., 2019). It should be noted that second-generation

https://doi.org/10.5194/acp-2022-85
Preprint. Discussion started: 4 February 2022

Atmospheric Chemistry and Physics Discussions

521 HOM which contributed greatly to the limonene + NO_3 reaction system is not included in this primary HOM yield.

522

523 **3.6 Contribution of HOM to particle formation and growth**

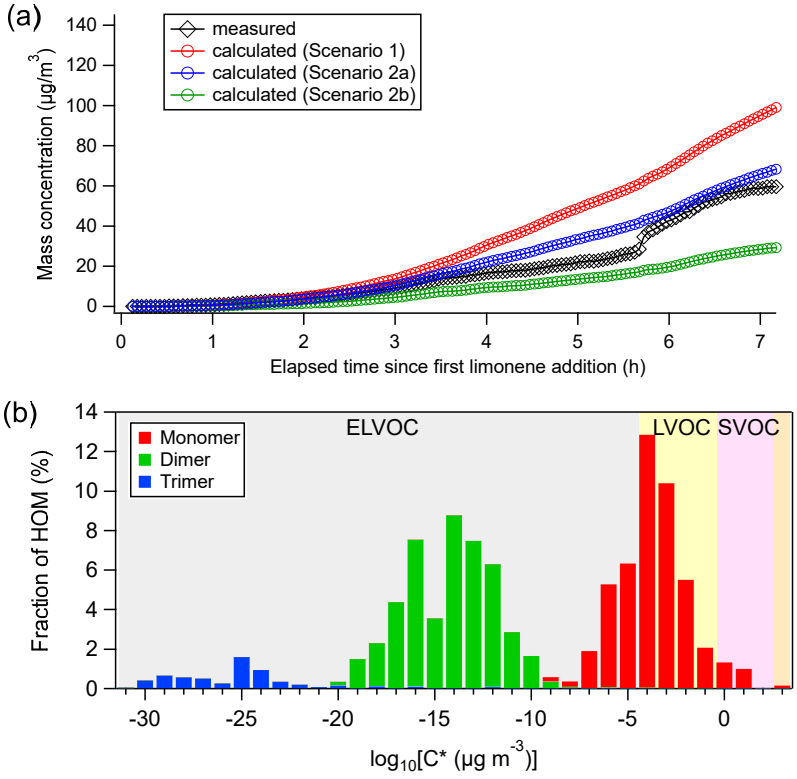

524

525 Figure 7. (a) Comparison of measured particle concentrations (black) with those predicted from condensation of
526 measured HOM on aerosol particles, where red markers were calculated under Scenario 1, blue and green markers
527 were calculated under Scenario 2 (only considering the condensation of ELVOC and LVOC) with the volatility
528 calculated using the method by Mohr et al. (2019) (Scenario 2a) and Peräkylä et al. (2020) (Scenario 2b)
529 respectively. (b) HOM volatility distribution using formula provided by Mohr et al. (2019). Average concentrations
530 of HOM in the P1 period were used to calculate the fraction of HOM.

531

532 We calculated the contribution of HOM to SOA formation and particle growth and compared it to the measured
533 particle growth (Fig. 7a). We assumed different scenarios of HOM uptake on aerosol particles, using the calculation
534 method in the literature (Ehn et al., 2014; Seinfeld and Pandis, 2006; Nieminen et al., 2010). The assumption that all

https://doi.org/10.5194/acp-2022-85
Preprint. Discussion started: 4 February 2022


Atmospheric Chemistry and Physics Discussions

535 HOM irreversibly condense on the particles (Scenario 1) resulted in a strong overestimation of particle mass growth
536 (red markers in Fig. 7a). Applying the parametrizations of Mohr et al. (2019) (Scenario 2a) or Peräkylä et al. (2020)
537 (Scenario 2b) for classification and accounting only LVOC- and ELVOC-HOM for irreversible uptake framed the
538 observed values (blue and green markers in Fig. 7a). While Scenario 2a agreed quite well with the observations and
539 only slightly overestimated SOA concentration after 7 h by +11%, Scenario 2b underestimated the SOA concentration
540 at the end by -53%. The agreement between the modeled and observed SOA concentration suggests that HOM,
541 especially LVOC- and ELVOC-HOM play a major role in SOA growth in this study. According to the work by Faxon
542 et al. (2018), many of the dimers are ELVOC due to their partitioning behavior. This is consistent with our calculation
543 result based on the method of Mohr et al. (2019).

544 We observed nucleation and SOA growth in the limonene + NO_3 reaction. Since neither SO_2 nor H_2SO_4 was
545 added in our experiment, NPF could be attributed to the nucleation initiated by HOM of low volatility. HOM trimers
546 with as many as 30 carbon atoms were identified in the early stage of this study, and their loss matched the time when
547 rapid formation of SOA occurred. Trimers identified in our experiment are classified as ELVOC, with much lower
548 volatility than monomers and dimers (Fig. 7b). In contrast, in an earlier experiment investigating the NO_3-initiated
549 oxidation of β-pinene also conducted in the SAPHIR chamber under similar conditions, particles were barely formed
550 (< 20 cm^{-3}) (Shen et al., 2021). As mentioned above, no trimer HOM products were observed in that study, and only
551 molecules with C≤20 were detected (Sect. 3.4). Therefore, NPF in our study was likely attributed to HOM trimers
552 since they have the strongest potential of initiating nucleation due to their much lower volatility compared to
553 monomers and dimers. Extremely low volatile organic vapors formed in α-pinene ozonolysis have been shown to
554 induce nucleation and drive initial particle growth (Tröstl et al., 2016; Kirkby et al., 2016). Since our experiment of
555 NO_3 oxidation of limonene was performed under near atmospheric conditions, such NPF events induced by the
556 oxidation of limonene by NO_3 could also occur in the ambient atmosphere. Several field observations have shown
557 NPF events taking place at nighttime where biogenic emissions dominate (Kammer et al., 2018; Huang et al., 2019).
558 The work by Ortega et al. (2012) demonstrated an important role of monoterpene ozonlysis products in nocturnal
559 NPF events in chamber experiments. In a previous laboratory study, limonene + NO_3 appears more effective at
560 initiating nucleation than the limonene + O_3 reaction (Fry et al., 2014), which supports that limonene + NO_3 can play
561 a significant role in nighttime nucleation. Our study suggests that NO_3 oxidation of limonene could contribute to the
562 nighttime NPF via HOM trimer formation. In contrast, we infer that NO_3 reactions with other monoterpenes
563 containing only one double bond such as α-pinene and β-pinene are less likely candidates for nighttime NPF, because
564 gas-phase trimers are not observed.

https://doi.org/10.5194/acp-2022-85
Preprint. Discussion started: 4 February 2022

Atmospheric Chemistry and Physics Discussions

565

566 **4 Conclusion and implications**

567 HOM formation in the reaction of limonene with NO_3 was investigated in the SAPHIR chamber. About 280 gas-
568 phase HOM products were identified, including monomers ($C_{6\text{-}10}$, $O_{6\text{-}16}$, $N_{0\text{-}3}$), dimers ($C_{17\text{-}20}$, $O_{7\text{-}20}$, $N_{0\text{-}4}$) and trimers
569 ($C_{27\text{-}30}$, $O_{16\text{-}25}$, $N_{1\text{-}6}$). Nitrogen-containing products dominated the HOM, with compounds of the $C_{10}H_{15\text{-}17}NO_{6\text{-}14}$
570 series being the most prevalent. Dimers contributed 47 % in the early stage of the experiment when new particle
571 formation (NPF) had not occurred yet, which was similar to monomers (47 %). Tentative formation pathways of
572 major families were proposed in this work based on their time-dependent concentration profiles.

573 In HOM monomers, the abundance of carbonyl compounds significantly exceeded that of hydroxyl or
574 hydroperoxy compounds, indicating the significance of unimolecular termination of HOM-RO_2 radicals. Both RO_2•
575 autoxidation and alkoxy-peroxy pathways were found to be important in the formation of HOM monomers.
576 Monomers with 1 nitrogen atom (1N-monomers) contained both first- and second-generation products, which could
577 be formed via NO_3 oxidation of limonene and its first-generation products with the latter being more important.
578 Monomers with 2 nitrogen atoms were classified as second-generation products, which could be formed via NO_3
579 oxidation of the remaining C=C double bond of 1N-monomers.

580 Dimers showed both first- and second-generation time pattern. Dimers were mostly formed via accretion
581 reactions between monomer RO_2 radicals, resulting in a decrease in O/C ratio compared to monomers. The initial
582 less oxygenated RO_2• such as $C_{10}H_{16}O_5$• likely played an important role in dimer formation based on the comparison
583 of expected dimer identity and concentrations according to accretion monomer RO_2• reactions with measured ones.
584 Trimers were likely formed via accretion reactions between monomer RO_2 and dimer RO_2 radicals. Trimer formation
585 is attributed to the two double bonds in limonene, which can first react with NO_3 leading to dimer products with
586 remaining C=C double bond, thus providing reactive site for further oxidation by NO_3 forming dimer RO_2 radicals.

587 NPF observed in this work was likely related to the trimer formation due to much lower volatility of trimers
588 compared to monomers and dimers. The SOA concentration in the limonene + NO_3 reaction could be explained by
589 the condensation of the HOM belonging to LVOC and ELVOC classes assuming irreversible uptake, suggesting the
590 important role of HOM for SOA growth in this reaction system.

591 A "primary" HOM molar yield of 1.5 $\%^{+1.7\ \%}_{-0.7\ \%}$ in the limonene + NO_3 reaction was estimated, which is much
592 lower than the total HOM yield in the reaction of limonene with ozone (5 to 17 %) (Ehn et al., 2014; Jokinen et al.,
593 2015; Pagonis et al., 2019). It is worth noting that only first-generation HOM were taken into consideration in our
594 calculation of HOM yield, while second-generation HOM contributed greatly to monomers, dimers and trimers, and

https://doi.org/10.5194/acp-2022-85
Preprint. Discussion started: 4 February 2022

Atmospheric Chemistry and Physics Discussions

595 hence the HOM yield we obtained is a lower limit of the total HOM yield.

596 To our knowledge, this work is the first identifying trimer products from the limonene + NO_3 reaction system,
597 suggesting that limonene + NO_3 is a possible crucial source of new particles formed in nighttime biogenic emission-
598 dominated areas (Kammer et al., 2018; Huang et al., 2019). Our work highlights the need to consider the role of
599 limonene + NO_3 in NPF in models simulating nighttime aerosols formation in biogenic-emission dominated areas,
600 especially with large limonene emission. In addition, comparison with the reactions of NO_3 with isoprene (Zhao et
601 al., 2021) and other monoterpenes (Shen et al., 2021) reveals a strong dependence of HOM products on VOC species
602 in NO_3-initiated chemistry.

603 The concentration of limonene and NO_3 in this study were on the order of few ppb and ~100 ppt, which is similar
604 to the ambient levels in forest regions affected by anthropogenic emissions (Brown and Stutz, 2012). The chemical
605 lifetime of NO_3 was on the order of 50 to 500 s, which is also similar to ambient conditions at nighttime (Fry et al.,
606 2018). The RO_2• loss pathway in our study was dominated by the reactions RO_2• + NO_3 and of RO_2• + RO_2•, which
607 is representative for the RO_2• fate in urban areas and forested areas influenced by an urban plume. Therefore, the
608 HOM products and their formation process in our study are representative for forested regions influenced by
609 anthropogenic plume and ambient urban regions with high volatile commercial products emissions as limonene is a
610 typical component of volatile chemical products (VCP) (Nazaroff and Weschler, 2004). In these regions, HOM from
611 monoterpene + NO_3 reactions can be major components of nighttime SOA.

612 This study also highlights the important role of second-generation chemistry in HOM formation, which needs
613 to be further investigated and should be included in chemical mechanism used in numerical models. Additional work
614 is also needed to investigate the role of different HOM formed via NO_3-initiated BVOC oxidation reactions in NPF
615 and SOA growth in order to better constrain the climatic and environmental effects of BVOC + NO_3 chemistry.

616

617 **Acknowledgement**

618 Y. Guo, H. Shen, H. Luo, and D. Zhao would like to thank the funding support of Science and Technology
619 Commission of Shanghai Municipality (No. 20230711400), National Natural Science Foundation of China (No.
620 41875145), and Shanghai International Science and Technology Partnership Project (No. 21230780200). Sungah
621 Kang, Astrid Kiendler-Scharr, and Thomas F. Mentel acknowledge the support by the EU Project FORCeS (grant
622 agreement no. 821205)

https://doi.org/10.5194/acp-2022-85
Preprint. Discussion started: 4 February 2022

Atmospheric Chemistry and Physics Discussions

References

Ayres, B. R., Allen, H. M., Draper, D. C., Brown, S. S., Wild, R. J., Jimenez, J. L., Day, D. A., Campuzano-Jost, P., Hu, W., de Gouw, J., Koss, A., Cohen, R. C., Duffey, K. C., Romer, P., Baumann, K., Edgerton, E., Takahama, S., Thornton, J. A., Lee, B. H., Lopez-Hilfiker, F. D., Mohr, C., Wennberg, P. O., Nguyen, T. B., Teng, A., Goldstein, A. H., Olson, K., and Fry, J. L.: Organic nitrate aerosol formation via NO_3 + biogenic volatile organic compounds in the southeastern United States, Atmos. Chem. Phys., 15, 13377-13392, 10.5194/acp-15-13377-2015, 2015.

Beaver, M. R., Clair, J. M. S., Paulot, F., Spencer, K. M., Crounse, J. D., LaFranchi, B. W., Min, K. E., Pusede, S. E., Wooldridge, P. J., Schade, G. W., Park, C., Cohen, R. C., and Wennberg, P. O.: Importance of biogenic precursors to the budget of organic nitrates: observations of multifunctional organic nitrates by CIMS and TD-LIF during BEARPEX 2009, Atmos. Chem. Phys., 12, 5773-5785, 10.5194/acp-12-5773-2012, 2012.

Bell, D. M., Wu, C., Bertrand, A., Graham, E., Schoonbaert, J., Giannoukos, S., Baltensperger, U., Prevot, A. S. H., Riipinen, I., El Haddad, I., and Mohr, C.: Particle-phase processing of α-pinene NO3 secondary organic aerosol in the dark, Atmos. Chem. Phys. Discuss., 2021, 1-28, 10.5194/acp-2021-379, 2021.

Berkemeier, T., Takeuchi, M., Eris, G., and Ng, N. L.: Kinetic modeling of formation and evaporation of secondary organic aerosol from NO_3 oxidation of pure and mixed monoterpenes, Atmos. Chem. Phys., 20, 15513-15535, 10.5194/acp-20-15513-2020, 2020.

Berndt, T., Mender, B., Scholz, W., Fischer, L., Herrmann, H., Kulmala, M., and Hansel, A.: Accretion Product Formation from Ozonolysis and OH Radical Reaction of α-Pinene: Mechanistic Insight and the Influence of Isoprene and Ethylene, Environ. Sci. Technol., 52, 11069-11077, 10.1021/acs.est.8b02210, 2018a.

Berndt, T., Scholz, W., Mentler, B., Fischer, L., Herrmann, H., Kulmala, M., and Hansel, A.: Accretion Product Formation from Self- and Cross-Reactions of RO_2 Radicals in the Atmosphere, Angew. Chem. Int. Edit., 57, 3820-3824, 10.1002/anie.201710989, 2018b.

Bianchi, F., Kurtén, T., Riva, M., Mohr, C., Rissanen, M. P., Roldin, P., Berndt, T., Crounse, J. D., Wennberg, P. O., Mentel, T. F., Wildt, J., Junninen, H., Jokinen, T., Kulmala, M., Worsnop, D. R., Thornton, J. A., Donahue, N., Kjaergaard, H. G., and Ehn, M.: Highly Oxygenated Organic Molecules (HOM) from Gas-Phase Autoxidation Involving Peroxy Radicals: A Key Contributor to Atmospheric Aerosol, Chem. Rev., 119, 3472-3509, 10.1021/acs.chemrev.8b00395, 2019.

Boyd, C. M., Nah, T., Xu, L., Berkemeier, T., and Ng, N. L.: Secondary Organic Aerosol (SOA) from Nitrate Radical Oxidation of Monoterpenes: Effects of Temperature, Dilution, and Humidity on Aerosol Formation, Mixing, and Evaporation, Environ. Sci. Technol., 51, 7831-7841, 10.1021/acs.est.7b01460, 2017.

Boyd, C. M., Sanchez, J., Xu, L., Eugene, A. J., Nah, T., Tuet, W. Y., Guzman, M. I., and Ng, N. L.: Secondary organic aerosol formation from the β-pinene+NO_3 system: effect of humidity and peroxy radical fate, Atmos. Chem. Phys., 15, 7497-7522, 10.5194/acp-15-7497-2015, 2015.

Brown, S. S. and Stutz, J.: Nighttime radical observations and chemistry, Chem. Soc. Rev., 41, 6405-6447, 10.1039/c2cs35181a, 2012.

Carslaw, N., Mota, T., Jenkin, M. E., Barley, M. H., and McFiggans, G.: A significant role for nitrate and peroxide groups on indoor secondary organic aerosol, Environ. Sci. Technol., 46, 9290-9298, 10.1021/es301350x, 2012.

Chen, Y., Takeuchi, M., Nah, T., Xu, L., Canagaratna, M. R., Stark, H., Baumann, K., Canonaco, F., Prévôt, A. S. H., Huey, L. G., Weber, R. J., and Ng, N. L.: Chemical characterization of secondary organic aerosol at a rural site in the southeastern US: insights from simultaneous high-resolution time-of-flight aerosol mass spectrometer (HR-ToF-AMS) and FIGAERO chemical ionization mass spectrometer (CIMS) measurements, Atmos. Chem. Phys., 20, 8421-8440, 10.5194/acp-20-8421-2020, 2020.

Claflin, M. S. and Ziemann, P. J.: Identification and Quantitation of Aerosol Products of the Reaction of β-Pinene with NO_3 Radicals and Implications for Gas- and Particle-Phase Reaction Mechanisms, J. Phys. Chem. A, 122, 3640-3652, 10.1021/acs.jpca.8b00692, 2018.

Clausen, P. A., Wilkins, C. K., Wolkoff, P., and Nielsen, G. D.: Chemical and biological evaluation of a reaction mixture of R-(+)-limonene/ozone - Formation of strong airway irritants, Environ. Int., 26, 511-522, 10.1016/s0160-4120(01)00035-6, 2001.

Crounse, J. D., Nielsen, L. B., Jørgensen, S., Kjaergaard, H. G., and Wennberg, P. O.: Autoxidation of Organic Compounds in the

https://doi.org/10.5194/acp-2022-85
Preprint. Discussion started: 4 February 2022

Atmospheric Chemistry and Physics Discussions

669 Atmosphere, J. Phys. Chem. Lett., 4, 3513-3520, 10.1021/jz4019207, 2013.
670 Donahue, N. M., Epstein, S. A., Pandis, S. N., and Robinson, A. L.: A two-dimensional volatility basis set: 1. organic-aerosol mixing
671 thermodynamics, Atmos. Chem. Phys., 11, 3303-3318, 10.5194/acp-11-3303-2011, 2011.
672 Donahue, N. M., Kroll, J. H., Pandis, S. N., and Robinson, A. L.: A two-dimensional volatility basis set – Part 2: Diagnostics of
673 organic-aerosol evolution, Atmos. Chem. Phys., 12, 615-634, 10.5194/acp-12-615-2012, 2012.
674 Ehn, M., Thornton, J. A., Kleist, E., Sipilä, M., Junninen, H., Pullinen, I., Springer, M., Rubach, F., Tillmann, R., Lee, B., Lopez-
675 Hilfiker, F., Andres, S., Acir, I. H., Rissanen, M., Jokinen, T., Schobesberger, S., Kangasluoma, J., Kontkanen, J., Nieminen,
676 T., Kurtén, T., Nielsen, L. B., Jørgensen, S., Kjaergaard, H. G., Canagaratna, M., Dal Maso, M., Berndt, T., Petäjä, T., Wahner,
677 A., Kerminen, V. M., Kulmala, M., Worsnop, D. R., Wildt, J., and Mentel, T. F.: A large source of low-volatility secondary
678 organic aerosol, Nature, 506, 476-485, 10.1038/nature13032, 2014.
679 Eisele, F. L. and Tanner, D. J.: Measurement of the gas phase concentration of H_2SO_4 and methane sulfonic acid and estimates of
680 H_2SO_4 production and loss in the atmosphere, J. Geophys. Res.-Atmos., 98, 9001-9010, 10.1029/93jd00031, 1993.
681 Fan, Z. H., Lioy, P., Weschler, C., Fiedler, N., Kipen, H., and Zhang, J. F.: Ozone-initiated reactions with mixtures of volatile organic
682 compounds under simulated indoor conditions, Environ. Sci. Technol., 37, 1811-1821, 10.1021/es026231i, 2003.
683 Faxon, C., Hammes, J., Le Breton, M., Pathak, R. K., and Hallquist, M.: Characterization of organic nitrate constituents of secondary
684 organic aerosol (SOA) from nitrate-radical-initiated oxidation of limonene using high-resolution chemical ionization mass
685 spectrometry, Atmos. Chem. Phys., 18, 5467-5481, 10.5194/acp-18-5467-2018, 2018.
686 Finlayson-Pitts, B. J. and Pitts, J. N.: Tropospheric air pollution: Ozone, airborne toxics, polycyclic aromatic hydrocarbons, and
687 particles, Science, 276, 1045-1052, 10.1126/science.276.5315.1045, 1997.
688 Fry, J. L., Draper, D. C., Barsanti, K. C., Smith, J. N., Ortega, J., Winkler, P. M., Lawler, M. J., Brown, S. S., Edwards, P. M., Cohen,
689 R. C., and Lee, L.: Secondary organic aerosol formation and organic nitrate yield from NO_3 oxidation of biogenic hydrocarbons,
690 Environ. Sci. Technol., 48, 11944-11953, 10.1021/es502204x, 2014.
691 Fry, J. L., Kiendler-Scharr, A., Rollins, A. W., Brauers, T., Brown, S. S., Dorn, H. P., Dubé, W. P., Fuchs, H., Mensah, A., Rohrer,
692 F., Tillmann, R., Wahner, A., Wooldridge, P. J., and Cohen, R. C.: SOA from limonene: role of NO_3 in its generation and
693 degradation, Atmos. Chem. Phys., 11, 3879-3894, 10.5194/acp-11-3879-2011, 2011.
694 Fry, J. L., Draper, D. C., Zarzana, K. J., Campuzano-Jost, P., Day, D. A., Jimenez, J. L., Brown, S. S., Cohen, R. C., Kaser, L.,
695 Hansel, A., Cappellin, L., Karl, T., Hodzic Roux, A., Turnipseed, A., Cantrell, C., Lefer, B. L., and Grossberg, N.: Observations
696 of gas- and aerosol-phase organic nitrates at BEACHON-RoMBAS 2011, Atmos. Chem. Phys., 13, 8585-8605, 10.5194/acp-
697 13-8585-2013, 2013.
698 Fry, J. L., Brown, S. S., Middlebrook, A. M., Edwards, P. M., Campuzano-Jost, P., Day, D. A., Jimenez, J. L., Allen, H. M., Ryerson,
699 T. B., Pollack, I., Graus, M., Warneke, C., de Gouw, J. A., Brock, C. A., Gilman, J., Lerner, B. M., Dubé, W. P., Liao, J., and
700 Welti, A.: Secondary organic aerosol (SOA) yields from NO_3 radical + isoprene based on nighttime aircraft power plant plume
701 transects, Atmos. Chem. Phys., 18, 11663-11682, 10.5194/acp-18-11663-2018, 2018.
702 Fuchs, N. A. and Sutugin, A. G.: Topics in Current Aerosol Research (Part 2), Pergamon, New York, 1971.
703 Gkatzelis, G. I., Coggon, M. M., McDonald, B. C., Peischl, J., Aikin, K. C., Gilman, J. B., Trainer, M., and Warneke, C.: Identifying
704 Volatile Chemical Product Tracer Compounds in U.S. Cities, Environ. Sci. Technol., 55, 188-199, 10.1021/acs.est.0c05467,
705 2021.
706 Guenther, A. B., Jiang, X., Heald, C. L., Sakulyanontvittaya, T., Duhl, T., Emmons, L. K., and Wang, X.: The Model of Emissions
707 of Gases and Aerosols from Nature version 2.1 (MEGAN2.1): an extended and updated framework for modeling biogenic
708 emissions, Geosci. Model Dev., 5, 1471-1492, 10.5194/gmd-5-1471-2012, 2012.
709 Hallquist, M., Wängberg, I., Ljungström, E., Barnes, I., and Becker, K. H.: Aerosol and product yields from NO_3 radical-initiated
710 oxidation of selected monoterpenes, Environ. Sci. Technol., 33, 553-559, 10.1021/es980292s, 1999.
711 Hallquist, M., Wenger, J. C., Baltensperger, U., Rudich, Y., Simpson, D., Claeys, M., Dommen, J., Donahue, N. M., George, C.,
712 Goldstein, A. H., Hamilton, J. F., Herrmann, H., Hoffmann, T., Iinuma, Y., Jang, M., Jenkin, M. E., Jimenez, J. L., Kiendler-
713 Scharr, A., Maenhaut, W., McFiggans, G., Mentel, T. F., Monod, A., Prévôt, A. S. H., Seinfeld, J. H., Surratt, J. D., Szmigielski,
714 R., and Wildt, J.: The formation, properties and impact of secondary organic aerosol: current and emerging issues, Atmos.
715 Chem. Phys., 9, 5155-5236, 10.5194/acp-9-5155-2009, 2009.

https://doi.org/10.5194/acp-2022-85
Preprint. Discussion started: 4 February 2022

716 Huang, W., Saathoff, H., Shen, X., Ramisetty, R., Leisner, T., and Mohr, C.: Chemical Characterization of Highly Functionalized
717 Organonitrates Contributing to Night-Time Organic Aerosol Mass Loadings and Particle Growth, Environ. Sci. Technol., 53,
718 1165-1174, 10.1021/acs.est.8b05826, 2019.
719 Jiang, L., Wang, W., and Xu, Y. S.: Theoretical investigation of the NO_3 radical addition to double bonds of limonene, Int. J. Mol.
720 Sci., 10, 3743-3754, 10.3390/ijms10093743, 2009.
721 Jokinen, T., Sipilä, M., Junninen, H., Ehn, M., Lönn, G., Hakala, J., Petäjä, T., Mauldin, R. L., Kulmala, M., and Worsnop, D. R.:
722 Atmospheric sulphuric acid and neutral cluster measurements using CI-APi-TOF, Atmos. Chem. Phys., 12, 4117-4125,
723 10.5194/acp-12-4117-2012, 2012.
724 Jokinen, T., Berndt, T., Makkonen, R., Kerminen, V. M., Junninen, H., Paasonen, P., Stratmann, F., Herrmann, H., Guenther, A. B.,
725 Worsnop, D. R., Kulmala, M., Ehn, M., and Sipilä, M.: Production of extremely low volatile organic compounds from biogenic
726 emissions: Measured yields and atmospheric implications, P. Natl. Acad. Sci. USA, 112, 7123-7128, 10.1073/pnas.1423977112,
727 2015.
728 Kammer, J., Perraudin, E., Flaud, P. M., Lamaud, E., Bonnefond, J. M., and Villenave, E.: Observation of nighttime new particle
729 formation over the French Landes forest, Sci. Total Environ., 621, 1084-1092, 10.1016/j.scitotenv.2017.10.118, 2018.
730 Kirkby, J., Duplissy, J., Sengupta, K., Frege, C., Gordon, H., Williamson, C., Heinritzi, M., Simon, M., Yan, C., Almeida, J., Tröstl,
731 J., Nieminen, T., Ortega, I. K., Wagner, R., Adamov, A., Amorim, A., Bernhammer, A. K., Bianchi, F., Breitenlechner, M.,
732 Brilke, S., Chen, X., Craven, J., Dias, A., Ehrhart, S., Flagan, R. C., Franchin, A., Fuchs, C., Guida, R., Hakala, J., Hoyle, C.
733 R., Jokinen, T., Junninen, H., Kangasluoma, J., Kim, J., Krapf, M., Kürten, A., Laaksonen, A., Lehtipalo, K., Makhmutov, V.,
734 Mathot, S., Molteni, U., Onnela, A., Peräkylä, O., Piel, F., Petäjä, T., Praplan, A. P., Pringle, K., Rap, A., Richards, N. A.,
735 Riipinen, I., Rissanen, M. P., Rondo, L., Sarnela, N., Schobesberger, S., Scott, C. E., Seinfeld, J. H., Sipilä, M., Steiner, G.,
736 Stozhkov, Y., Stratmann, F., Tomé, A., Virtanen, A., Vogel, A. L., Wagner, A. C., Wagner, P. E., Weingartner, E., Wimmer, D.,
737 Winkler, P. M., Ye, P., Zhang, X., Hansel, A., Dommen, J., Donahue, N. M., Worsnop, D. R., Baltensperger, U., Kulmala, M.,
738 Carslaw, K. S., and Curtius, J.: Ion-induced nucleation of pure biogenic particles, Nature, 533, 521-526, 10.1038/nature17953,
739 2016.
740 Klinger, L. F., Li, Q. J., Guenther, A. B., Greenberg, J. P., Baker, B., and Bai, J. H.: Assessment of volatile organic compound
741 emissions from ecosystems of China, J. Geophys. Res.-Atmos., 107, 10.1029/2001jd001076, 2002.
742 Kurtén, T., Møller, K. H., Nguyen, T. B., Schwantes, R. H., Misztal, P. K., Su, L., Wennberg, P. O., Fry, J. L., and Kjaergaard, H.
743 G.: Alkoxy Radical Bond Scissions Explain the Anomalously Low Secondary Organic Aerosol and Organonitrate Yields From
744 α-Pinene + NO_3, J. Phys. Chem. Lett., 8, 2826-2834, 10.1021/acs.jpclett.7b01038, 2017.
745 Lee, B. H., Mohr, C., Lopez-Hilfiker, F. D., Lutz, A., Hallquist, M., Lee, L., Romer, P., Cohen, R. C., Iyer, S., Kurten, T., Hu, W.,
746 Day, D. A., Campuzano-Jost, P., Jimenez, J. L., Xu, L., Ng, N. L., Guo, H., Weber, R. J., Wild, R. J., Brown, S. S., Koss, A., de
747 Gouw, J., Olson, K., Goldstein, A. H., Seco, R., Kim, S., McAvey, K., Shepson, P. B., Starn, T., Baumann, K., Edgerton, E. S.,
748 Liu, J., Shilling, J. E., Miller, D. O., Brune, W., Schobesberger, S., D'Ambro, E. L., and Thornton, J. A.: Highly functionalized
749 organic nitrates in the southeast United States: Contribution to secondary organic aerosol and reactive nitrogen budgets, P. Natl.
750 Acad. Sci. USA, 113, 1516-1521, 10.1073/pnas.1508108113, 2016.
751 Massoli, P., Stark, H., Canagaratna, M. R., Krechmer, J. E., Xu, L., Ng, N. L., Mauldin, R. L., Yan, C., Kimmel, J., Misztal, P. K.,
752 Jimenez, J. L., Jayne, J. T., and Worsnop, D. R.: Ambient Measurements of Highly Oxidized Gas-Phase Molecules during the
753 Southern Oxidant and Aerosol Study (SOAS) 2013, ACS Earth and Space Chemistry, 2, 653-672,
754 10.1021/acsearthspacechem.8b00028, 2018.
755 McDonald, B. C., de Gouw, J. A., Gilman, J. B., Jathar, S. H., Akherati, A., Cappa, C. D., Jimenez, J. L., Lee-Taylor, J., Hayes, P.
756 L., McKeen, S. A., Cui, Y. Y., Kim, S.-W., Gentner, D. R., Isaacman-VanWertz, G., Goldstein, A. H., Harley, R. A., Frost, G.
757 J., Roberts, J. M., Ryerson, T. B., and Trainer, M.: Volatile chemical products emerging as largest petrochemical source of
758 urban organic emissions, Science, 359, 760-764, 10.1126/science.aaq0524, 2018.
759 McFiggans, G., Mentel, T. F., Wildt, J., Pullinen, I., Kang, S., Kleist, E., Schmitt, S., Springer, M., Tillmann, R., Wu, C., Zhao, D.
760 F., Hallquist, M., Faxon, C., Le Breton, M., Hallquist, A. M., Simpson, D., Bergström, R., Jenkin, M. E., Ehn, M., Thornton, J.
761 A., Alfarra, M. R., Bannan, T. J., Percival, C. J., Priestley, M., Topping, D., and Kiendler-Scharr, A.: Secondary organic aerosol
762 reduced by mixture of atmospheric vapours, Nature, 565, 587-593, 10.1038/s41586-018-0871-y, 2019.

https://doi.org/10.5194/acp-2022-85
Preprint. Discussion started: 4 February 2022

Atmospheric Chemistry and Physics Discussions

763 Mentel, T. F., Springer, M., Ehn, M., Kleist, E., Pullinen, I., Kurtén, T., Rissanen, M., Wahner, A., and Wildt, J.: Formation of highly
764 oxidized multifunctional compounds: autoxidation of peroxy radicals formed in the ozonolysis of alkenes – deduced from
765 structure–product relationships, Atmos. Chem. Phys., 15, 6745-6765, 10.5194/acp-15-6745-2015, 2015.
766 Mohr, C., Thornton, J. A., Heitto, A., Lopez-Hilfiker, F. D., Lutz, A., Riipinen, I., Hong, J., Donahue, N. M., Hallquist, M., Petäjä,
767 T., Kulmala, M., and Yli-Juuti, T.: Molecular identification of organic vapors driving atmospheric nanoparticle growth, Nat.
768 Commun., 10, 4442, https://doi.org/10.1038/s41467-019-12473-2, 2019.
769 Mutzel, A., Zhang, Y., Böge, O., Rodigast, M., Kolodziejczyk, A., Wang, X., and Herrmann, H.: Importance of secondary organic
770 aerosol formation of α-pinene, limonene, and m-cresol comparing day- and nighttime radical chemistry, Atmos. Chem. Phys.,
771 21, 8479-8498, 10.5194/acp-21-8479-2021, 2021.
772 Nah, T., Sanchez, J., Boyd, C. M., and Ng, N. L.: Photochemical Aging of α-pinene and β-pinene Secondary Organic Aerosol formed
773 from Nitrate Radical Oxidation, Environ. Sci. Technol., 50, 222-231, 10.1021/acs.est.5b04594, 2016.
774 Nazaroff, W. W. and Weschler, C. J.: Cleaning products and air fresheners: exposure to primary and secondary air pollutants, Atmos.
775 Environ., 38, 2841-2865, 10.1016/j.atmosenv.2004.02.040, 2004.
776 Ng, N. L., Kwan, A. J., Surratt, J. D., Chan, A. W. H., Chhabra, P. S., Sorooshian, A., Pye, H. O. T., Crounse, J. D., Wennberg, P. O.,
777 Flagan, R. C., and Seinfeld, J. H.: Secondary organic aerosol (SOA) formation from reaction of isoprene with nitrate radicals
778 (NO_3), Atmos. Chem. Phys., 8, 4117-4140, 10.5194/acp-8-4117-2008, 2008.
779 Nieminen, T., Lehtinen, K. E. J., and Kulmala, M.: Sub-10 nm particle growth by vapor condensation – effects of vapor molecule
780 size and particle thermal speed, Atmos. Chem. Phys., 10, 9773-9779, 10.5194/acp-10-9773-2010, 2010.
781 Novelli, A., Cho, C., Fuchs, H., Hofzumahaus, A., Rohrer, F., Tillmann, R., Kiendler-Scharr, A., Wahner, A., and Vereecken, L.:
782 Experimental and theoretical study on the impact of a nitrate group on the chemistry of alkoxy radicals, Phys. Chem. Chem.
783 Phys., 23, 5474-5495, 10.1039/d0cp05555g, 2021.
784 Ortega, I. K., Suni, T., Boy, M., Grönholm, T., Manninen, H. E., Nieminen, T., Ehn, M., Junninen, H., Hakola, H., Hellén, H.,
785 Valmari, T., Arvela, H., Zegelin, S., Hughes, D., Kitchen, M., Cleugh, H., Worsnop, D. R., Kulmala, M., and Kerminen, V. M.:
786 New insights into nocturnal nucleation, Atmos. Chem. Phys., 12, 4297-4312, 10.5194/acp-12-4297-2012, 2012.
787 Pagonis, D., Algrim, L. B., Price, D. J., Day, D. A., Handschy, A. V., Stark, H., Miller, S. L., de Gouw, J. A., Jimenez, J. L., and
788 Ziemann, P. J.: Autoxidation of Limonene Emitted in a University Art Museum, Environ. Sci. Tech. Let., 6, 520-524,
789 10.1021/acs.estlett.9b00425, 2019.
790 Peng, C., Wang, W., Li, K., Li, J., Zhou, L., Wang, L., and Ge, M.: The Optical Properties of Limonene Secondary Organic Aerosols:
791 The Role of NO3, OH, and O3 in the Oxidation Processes, J. Geophys. Res.-Atmos., 123, 3292-3303,
792 https://doi.org/10.1002/2017JD028090, 2018.
793 Peräkylä, O., Riva, M., Heikkinen, L., Quéléver, L., Roldin, P., and Ehn, M.: Experimental investigation into the volatilities of
794 highly oxygenated organic molecules (HOMs), Atmos. Chem. Phys., 20, 649-669, 10.5194/acp-20-649-2020, 2020.
795 Pullinen, I., Schmitt, S., Kang, S., Sarrafzadeh, M., Schlag, P., Andres, S., Kleist, E., Mentel, T. F., Rohrer, F., Springer, M., Tillmann,
796 R., Wildt, J., Wu, C., Zhao, D., Wahner, A., and Kiendler-Scharr, A.: Impact of NO_x on secondary organic aerosol (SOA)
797 formation from α-pinene and β-pinene photooxidation: the role of highly oxygenated organic nitrates, Atmos. Chem. Phys., 20,
798 10125-10147, 10.5194/acp-20-10125-2020, 2020.
799 Pye, H. O. T., Chan, A. W. H., Barkley, M. P., and Seinfeld, J. H.: Global modeling of organic aerosol: the importance of reactive
800 nitrogen (NO_x and NO_3), Atmos. Chem. Phys., 10, 11261-11276, 10.5194/acp-10-11261-2010, 2010.
801 Rissanen, M. P., Kurtén, T., Sipilä, M., Thornton, J. A., Kangasluoma, J., Sarnela, N., Junninen, H., Jørgensen, S., Schallhart, S.,
802 Kajos, M. K., Taipale, R., Springer, M., Mentel, T. F., Ruuskanen, T., Petäjä, T., Worsnop, D. R., Kjaergaard, H. G., and Ehn,
803 M.: The formation of highly oxidized multifunctional products in the ozonolysis of cyclohexene, J. Am. Chem. Soc., 136,
804 15596-15606, 10.1021/ja507146s, 2014.
805 Riva, M., Heikkinen, L., Bell, D. M., Peräkylä, O., Zha, Q., Schallhart, S., Rissanen, M. P., Imre, D., Petäjä, T., Thornton, J. A.,
806 Zelenyuk, A., and Ehn, M.: Chemical transformations in monoterpene-derived organic aerosol enhanced by inorganic
807 composition, Npj Climate and Atmospheric Science, 2, 10.1038/s41612-018-0058-0, 2019.
808 Rohrer, F., Bohn, B., Brauers, T., Brüning, D., Johnen, F. J., Wahner, A., and Kleffmann, J.: Characterisation of the photolytic
809 HONO-source in the atmosphere simulation chamber SAPHIR, Atmos. Chem. Phys., 5, 2189-2201, 10.5194/acp-5-2189-2005,

https://doi.org/10.5194/acp-2022-85
Preprint. Discussion started: 4 February 2022

2005.

Rollins, A. W., Kiendler-Scharr, A., Fry, J. L., Brauers, T., Brown, S. S., Dorn, H. P., Dubé, W. P., Fuchs, H., Mensah, A., Mentel, T. F., Rohrer, F., Tillmann, R., Wegener, R., Wooldridge, P. J., and Cohen, R. C.: Isoprene oxidation by nitrate radical: alkyl nitrate and secondary organic aerosol yields, Atmos. Chem. Phys., 9, 6685-6703, 10.5194/acp-9-6685-2009, 2009.

Rollins, A. W. B., E. C.; Min, K.-E.; Pusede, S. E.; Wooldridge, P. J.; Gentner, D. R.; Goldstein, A. H.; Liu, S.; Day, D. A.; Russell, L. M.; Cohen, R. C.: Evidence for NO_x control over nighttime SOA formation, Science, 337, 1210-1212, 10.1126/science.1221520, 2012.

Saunders, S. M., Jenkin, M. E., Derwent, R. G., and Pilling, M. J.: Protocol for the development of the Master Chemical Mechanism, MCM v3 (Part A): tropospheric degradation of non-aromatic volatile organic compounds, Atmos. Chem. Phys., 3, 161-180, 10.5194/acp-3-161-2003, 2003.

Seinfeld, J. H. and Pandis, S. N.: Atmospheric Chemistry and Physics: From Air Pollution to Climate Change, 2nd ed, Wiley, John & Sons, New York, 2006.

Shen, H., Zhao, D., Pullinen, I., Kang, S., Vereecken, L., Fuchs, H., Acir, I.-H., Tillmann, R., Rohrer, F., Wildt, J., Kiendler-Scharr, A., Wahner, A., and Mentel, T. F.: Highly Oxygenated Organic Nitrates Formed from NO_3 Radical-Initiated Oxidation of β-Pinene, Environ. Sci. Technol., 10.1021/acs.est.1c03978, 2021.

Shrivastava, M., Cappa, C. D., Fan, J., Goldstein, A. H., Guenther, A. B., Jimenez, J. L., Kuang, C., Laskin, A., Martin, S. T., Ng, N. L., Petäjä, T., Pierce, J. R., Rasch, P. J., Roldin, P., Seinfeld, J. H., Shilling, J., Smith, J. N., Thornton, J. A., Volkamer, R., Wang, J., Worsnop, D. R., Zaveri, R. A., Zelenyuk, A., and Zhang, Q.: Recent advances in understanding secondary organic aerosol: Implications for global climate forcing, Rev. Geophys., 55, 509-559, 10.1002/2016rg000540, 2017.

Slade, J. H., de Perre, C., Lee, L., and Shepson, P. B.: Nitrate radical oxidation of γ-terpinene: hydroxy nitrate, total organic nitrate, and secondary organic aerosol yields, Atmos. Chem. Phys., 17, 8635-8650, 10.5194/acp-17-8635-2017, 2017.

Spittler, M., Barnes, I., Bejan, I., Brockmann, K. J., Benter, T., and Wirtz, K.: Reactions of NO_3 radicals with limonene and α-pinene: Product and SOA formation, Atmos. Environ., 40, 116-127, 10.1016/j.atmosenv.2005.09.093, 2006.

Takeuchi, M. and Ng, N. L.: Chemical composition and hydrolysis of organic nitrate aerosol formed from hydroxyl and nitrate radical oxidation of α-pinene and β-pinene, Atmos. Chem. Phys., 19, 12749-12766, 10.5194/acp-19-12749-2019, 2019.

Tröstl, J., Chuang, W. K., Gordon, H., Heinritzi, M., Yan, C., Molteni, U., Ahlm, L., Frege, C., Bianchi, F., Wagner, R., Simon, M., Lehtipalo, K., Williamson, C., Craven, J. S., Duplissy, J., Adamov, A., Almeida, J., Bernhammer, A. K., Breitenlechner, M., Brilke, S., Dias, A., Ehrhart, S., Flagan, R. C., Franchin, A., Fuchs, C., Guida, R., Gysel, M., Hansel, A., Hoyle, C. R., Jokinen, T., Junninen, H., Kangasluoma, J., Keskinen, H., Kim, J., Krapf, M., Kürten, A., Laaksonen, A., Lawler, M., Leiminger, M., Mathot, S., Möhler, O., Nieminen, T., Onnela, A., Petäjä, T., Piel, F. M., Miettinen, P., Rissanen, M. P., Rondo, L., Sarnela, N., Schobesberger, S., Sengupta, K., Sipilä, M., Smith, J. N., Steiner, G., Tomè, A., Virtanen, A., Wagner, A. C., Weingartner, E., Wimmer, D., Winkler, P. M., Ye, P., Carslaw, K. S., Curtius, J., Dommen, J., Kirkby, J., Kulmala, M., Riipinen, I., Worsnop, D. R., Donahue, N. M., and Baltensperger, U.: The role of low-volatility organic compounds in initial particle growth in the atmosphere, Nature, 533, 527-531, 10.1038/nature18271, 2016.

Vereecken, L. and Nozière, B.: H migration in peroxy radicals under atmospheric conditions, Atmos. Chem. Phys., 20, 7429-7458, 10.5194/acp-20-7429-2020, 2020.

Vereecken, L. and Peeters, J.: A structure-activity relationship for the rate coefficient of H-migration in substituted alkoxy radicals, Phys. Chem. Chem. Phys., 12, 12608-12620, 10.1039/c0cp00387e, 2010.

Wagner, N. L., Dubé, W. P., Washenfelder, R. A., Young, C. J., Pollack, I. B., Ryerson, T. B., and Brown, S. S.: Diode laser-based cavity ring-down instrument for NO_3, N_2O_5, NO, NO_2 and O_3 from aircraft, Atmos. Meas. Tech., 4, 1227-1240, 10.5194/amt-4-1227-2011, 2011.

Wang, S. and Pratt, K. A.: Molecular Halogens Above the Arctic Snowpack: Emissions, Diurnal Variations, and Recycling Mechanisms, J. Geophys. Res.-Atmos., 122, 11991-12007, 10.1002/2017jd027175, 2017.

Wu, C., Bell, D. M., Graham, E. L., Haslett, S., Riipinen, I., Baltensperger, U., Bertrand, A., Giannoukos, S., Schoonbaert, J., El Haddad, I., Prevot, A. S. H., Huang, W., and Mohr, C.: Photolytically induced changes in composition and volatility of biogenic secondary organic aerosol from nitrate radical oxidation during night-to-day transition, Atmos. Chem. Phys., 21, 14907-14925, 10.5194/acp-21-14907-2021, 2021a.

https://doi.org/10.5194/acp-2022-85
Preprint. Discussion started: 4 February 2022

Atmospheric Chemistry and Physics Discussions

857 Wu, R., Vereecken, L., Tsiligiannis, E., Kang, S., Albrecht, S. R., Hantschke, L., Zhao, D., Novelli, A., Fuchs, H., Tillmann, R.,
858 Hohaus, T., Carlsson, P. T. M., Shenolikar, J., Bernard, F., Crowley, J. N., Fry, J. L., Brownwood, B., Thornton, J. A., Brown,
859 S. S., Kiendler-Scharr, A., Wahner, A., Hallquist, M., and Mentel, T. F.: Molecular composition and volatility of multi-
860 generation products formed from isoprene oxidation by nitrate radical, Atmos. Chem. Phys., 21, 10799-10824, 10.5194/acp-
861 21-10799-2021, 2021b.
862 Xu, L., Guo, H., Boyd, C. M., Klein, M., Bougiatioti, A., Cerully, K. M., Hite, J. R., Isaacman-VanWertz, G., Kreisberg, N. M.,
863 Knote, C., Olson, K., Koss, A., Goldstein, A. H., Hering, S. V., de Gouw, J., Baumann, K., Lee, S.-H., Nenes, A., Weber, R. J.,
864 and Ng, N. L.: Effects of anthropogenic emissions on aerosol formation from isoprene and monoterpenes in the southeastern
865 United States, P. Natl. Acad. Sci. USA, 112, 37-42, 10.1073/pnas.1417609112, 2015.
866 Zhang, H., Yee, L. D., Lee, B. H., Curtis, M. P., Worton, D. R., Isaacman-VanWertz, G., Offenberg, J. H., Lewandowski, M.,
867 Kleindienst, T. E., Beaver, M. R., Holder, A. L., Lonneman, W. A., Docherty, K. S., Jaoui, M., Pye, H. O. T., Hu, W., Day, D.
868 A., Campuzano-Jost, P., Jimenez, J. L., Guo, H., Weber, R. J., de Gouw, J., Koss, A. R., Edgerton, E. S., Brune, W., Mohr, C.,
869 Lopez-Hilfiker, F. D., Lutz, A., Kreisberg, N. M., Spielman, S. R., Hering, S. V., Wilson, K. R., Thornton, J. A., and Goldstein,
870 A. H.: Monoterpenes are the largest source of summertime organic aerosol in the southeastern United States, P. Natl. Acad. Sci.
871 USA, 115, 2038-2043, 10.1073/pnas.1717513115, 2018.
872 Zhao, D., Pullinen, I., Fuchs, H., Schrade, S., Wu, R., Acir, I.-H., Tillmann, R., Rohrer, F., Wildt, J., Guo, Y., Kiendler-Scharr, A.,
873 Wahner, A., Kang, S., Vereecken, L., and Mentel, T. F.: Highly oxygenated organic molecule (HOM) formation in the isoprene
874 oxidation by NO_3 radical, Atmos. Chem. Phys., 21, 9681-9704, 10.5194/acp-21-9681-2021, 2021.
875 Zhao, D., Schmitt, S. H., Wang, M., Acir, I.-H., Tillmann, R., Tan, Z., Novelli, A., Fuchs, H., Pullinen, I., Wegener, R., Rohrer, F.,
876 Wildt, J., Kiendler-Scharr, A., Wahner, A., and Mentel, T. F.: Effects of NO_x and SO_2 on the secondary organic aerosol formation
877 from photooxidation of α-pinene and limonene, Atmos. Chem. Phys., 18, 1611-1628, 10.5194/acp-18-1611-2018, 2018.
878 Zhao, D. F., Buchholz, A., Kortner, B., Schlag, P., Rubach, F., Kiendler-Scharr, A., Tillmann, R., Wahner, A., Flores, J. M., Rudich,
879 Y., Watne, Å. K., Hallquist, M., Wildt, J., and Mentel, T. F.: Size-dependent hygroscopicity parameter (κ) and chemical
880 composition of secondary organic cloud condensation nuclei, Geophys. Res. Lett., 42, 10920-10928, 10.1002/2015gl066497,
881 2015a.
882 Zhao, D. F., Kaminski, M., Schlag, P., Fuchs, H., Acir, I. H., Bohn, B., Häseler, R., Kiendler-Scharr, A., Rohrer, F., Tillmann, R.,
883 Wang, M. J., Wegener, R., Wildt, J., Wahner, A., and Mentel, T. F.: Secondary organic aerosol formation from hydroxyl radical
884 oxidation and ozonolysis of monoterpenes, Atmos. Chem. Phys., 15, 991-1012, 10.5194/acp-15-991-2015, 2015b.
885 Zhou, L., Gierens, R., Sogachev, A., Mogensen, D., Ortega, J., Smith, J. N., Harley, P. C., Prenni, A. J., Levin, E. J. T., Turnipseed,
886 A., Rusanen, A., Smolander, S., Guenther, A. B., Kulmala, M., Karl, T., and Boy, M.: Contribution from biogenic organic
887 compounds to particle growth during the 2010 BEACHON-ROCS campaign in a Colorado temperate needleleaf forest, Atmos.
888 Chem. Phys., 15, 8643-8656, 10.5194/acp-15-8643-2015, 2015.
889 Ziemann, P. J. and Atkinson, R.: Kinetics, products, and mechanisms of secondary organic aerosol formation, Chem. Soc. Rev., 41,
890 6582-6605, 10.1039/c2cs35122f, 2012.
891